

AD-A115 119

ROCKWELL INTERNATIONAL THOUSAND OAKS CA SCIENCE CENTER F/O 6/11
IMPEDANCE MEASUREMENT FOR THE ANALYSIS OF CORROSION INDUCED FAI--ETC(U)
FEB 82 F B HANFELD, M W KENDIS N62269-80-C-0291

UNCLASSIFIED

NADC-80102-60

NL

101
A115

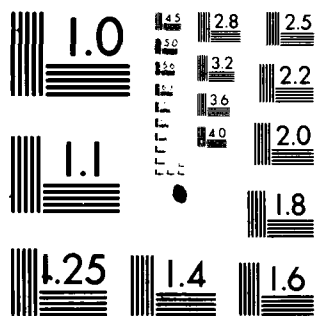
END

DATE

FILED

7-82

DTIC



MICROCOPY RESOLUTION TEST CHART
NATIONAL BUREAU OF STANDARDS 1963-A

REPORT NO. NADC-80102-60



IMPEDANCE MEASUREMENT FOR THE ANALYSIS
OF CORROSION INDUCED FAILURES

Florian B. Mansfeld and Martin W. Kendig
Rockwell International Science Center
1049 Camino Dos Rios
Thousand Oaks, California 91360

February 1982

FINAL REPORT
TASK AREA WR02201-001
Work Unit DG212

DTIC
S
JUN 3 1982
A

APPROVED FOR PUBLIC RELEASE; DISTRIBUTION UNLIMITED

Prepared for
United States Navy
NAVAL AIR DEVELOPMENT CENTER
Warminster, Pennsylvania 18974

DTIC FILE COPY

AD A115114

NOTICES

REPORT NUMBERING SYSTEM - The numbering of technical project reports issued by the Naval Air Development Center is arranged for specific identification purposes. Each number consists of the Center acronym, the calendar year in which the number was assigned, the sequence number of the report within the specific calendar year, and the official 2-digit correspondence code of the Command Office or the Functional Directorate responsible for the report. For example: Report No. NADC-78015-20 indicates the fifteenth Center report for the year 1978, and prepared by the Systems Directorate. The numerical codes are as follows:

CODE	OFFICE OR DIRECTORATE
00	Commander, Naval Air Development Center
01	Technical Director, Naval Air Development Center
02	Comptroller
10	Directorate Command Projects
20	Systems Directorate
30	Sensors & Avionics Technology Directorate
40	Communication & Navigation Technology Directorate
50	Software Computer Directorate
60	Aircraft & Crew Systems Technology Directorate
70	Planning Assessment Resources
80	Engineering Support Group

PRODUCT ENDORSEMENT - The discussion or instructions concerning commercial products herein do not constitute an endorsement by the Government nor do they convey or imply the license or right to use such products.

APPROVED BY:


J. R. WOODS
CDR, USN

DATE

4/26/82

UNCLASSIFIED

SECURITY CLASSIFICATION OF THIS PAGE (When Data Entered)

REPORT DOCUMENTATION PAGE		READ INSTRUCTIONS BEFORE COMPLETING FORM
1. REPORT NUMBER NADC-80102-60	2. GOVT ACCESSION NO.	3. RECIPIENT'S CATALOG NUMBER
4. TITLE (and Subtitle) IMPEDANCE MEASUREMENTS FOR THE ANALYSIS OF CORROSION INDUCED FAILURE		5. TYPE OF REPORT & PERIOD COVERED Final Report for the period 9/30/80 through 9/29/81
		6. PERFORMING ORG. REPORT NUMBER SC5287.5FR
7. AUTHOR(s) Florian B. Mansfeld and Martin W. Kendig		8. CONTRACT OR GRANT NUMBER(s) N62269-80-C-0291 <i>Contract is unclassified - PB</i>
9. PERFORMING ORGANIZATION NAME AND ADDRESS Rockwell International Science Center 1049 Camino Dos Rios Thousand Oaks, CA 91360		10. PROGRAM ELEMENT, PROJECT, TASK AREA & WORK UNIT NUMBERS
11. CONTROLLING OFFICE NAME AND ADDRESS NAVAL AIR DEVELOPMENT CENTER AIRCRAFT AND CREW SYSTEMS TECHNOLOGY DIRECTORATE WARMINSTER, PA 18974		12. REPORT DATE February, 1982
		13. NUMBER OF PAGES 56
14. MONITORING AGENCY NAME & ADDRESS (if different from Controlling Office)		15. SECURITY CLASS. (of this report) UNCLASSIFIED
		15a. DECLASSIFICATION/DOWNGRADING SCHEDULE
16. DISTRIBUTION STATEMENT (of this Report) APPROVED FOR PUBLIC RELEASE; DISTRIBUTION UNLIMITED		
17. DISTRIBUTION STATEMENT (of the abstract entered in Block 20, if different from Report)		
18. SUPPLEMENTARY NOTES		
19. KEY WORDS (Continue on reverse side if necessary and identify by block number) Stress corrosion cracking, corrosion fatigue, steel, aluminum, ac impedance, polarization curves, constant extension rate tests, passivation.		
20. ABSTRACT (Continue on reverse side if necessary and identify by block number) Electrochemical techniques for predicting stress corrosion cracking (SCC) susceptibility have been evaluated and constant extension rate tests (CERT) have been performed for a C-Mn Steel (C1117) in 1 M Na ₃ PO ₄ , pH=4, T=21 C and in 1.0 M NaHCO ₃ /0.1 M Na ₂ CO ₃ , T=70 C at controlled potentials with continuous recording of the a.c. impedance in a frequency range between 10 kHz and 30 mHz. These tests have been carried out in potential regions of susceptibili- ty to SCC which were determined by comparing fast and slow anodic potentio-		

DD FORM 1 JAN 73 1473

EDITION OF 1 NOV 65 IS OBSOLETE

UNCLASSIFIED

SECURITY CLASSIFICATION OF THIS PAGE (When Data Entered)

UNCLASSIFIED

SECURITY CLASSIFICATION OF THIS PAGE(When Data Entered)

dynamic polarization curves as suggested by Parkins and by analysis of a.c. impedance data as suggested by Armstrong. The occurrence of a high frequency relaxation phenomenon at the potential region where maximum susceptibility to SCC is observed seems to indicate that impedance spectra can be used to assess the SCC behavior. A model for the surface reactions occurring during CERT and the resulting impedance behavior is discussed.

UNCLASSIFIED

SECURITY CLASSIFICATION OF THIS PAGE(When Data Entered)

FORWARD

This report was prepared by Rockwell International Science Center, Thousand Oaks, California, for the Materials Protection Branch, Aero Materials Division, Aircraft and Crew Systems Technology Directorate of the Naval Air Development Center (NAVAIRDEVCECN), Warminster, Pennsylvania, under contract No. N62269-80-C-0291. Dr. Vinod S. Agarwala, Code 6062 was the project engineer and monitor.

The responsibility for performance of this program was given to the Corrosion and Environmental Effect Group of Rockwell International Science Center. Drs. F. B. Mansfeld and M. W. Kendig of Rockwell were the principal and associate investigators of the program respectively.

This report was released by the author in February, 1982 and covers the work accomplished during the period of September 1980 through September 1981.

Accession For

1915 1916 1917 1918 1919 1920 1921 1922 1923 1924 1925 1926 1927 1928 1929 1930 1931 1932 1933 1934 1935 1936 1937 1938 1939 1940 1941 1942 1943 1944 1945 1946 1947 1948 1949 1950 1951 1952 1953 1954 1955 1956 1957 1958 1959 1960 1961 1962 1963 1964 1965 1966 1967 1968 1969 1970 1971 1972 1973 1974 1975 1976 1977 1978 1979 1980 1981 1982 1983 1984 1985 1986 1987 1988 1989 1990 1991 1992 1993 1994 1995 1996 1997 1998 1999 2000 2001 2002 2003 2004 2005 2006 2007 2008 2009 2010 2011 2012 2013 2014 2015 2016 2017 2018 2019 2020 2021 2022 2023 2024 2025 2026 2027 2028 2029 2030 2031 2032 2033 2034 2035 2036 2037 2038 2039 2040 2041 2042 2043 2044 2045 2046 2047 2048 2049 2050 2051 2052 2053 2054 2055 2056 2057 2058 2059 2060 2061 2062 2063 2064 2065 2066 2067 2068 2069 2070 2071 2072 2073 2074 2075 2076 2077 2078 2079 2080 2081 2082 2083 2084 2085 2086 2087 2088 2089 2090 2091 2092 2093 2094 2095 2096 2097 2098 2099 2100 2101 2102 2103 2104 2105 2106 2107 2108 2109 2110 2111 2112 2113 2114 2115 2116 2117 2118 2119 2120 2121 2122 2123 2124 2125 2126 2127 2128 2129 2130 2131 2132 2133 2134 2135 2136 2137 2138 2139 2140 2141 2142 2143 2144 2145 2146 2147 2148 2149 2150 2151 2152 2153 2154 2155 2156 2157 2158 2159 2160 2161 2162 2163 2164 2165 2166 2167 2168 2169 2170 2171 2172 2173 2174 2175 2176 2177 2178 2179 2180 2181 2182 2183 2184 2185 2186 2187 2188 2189 2190 2191 2192 2193 2194 2195 2196 2197 2198 2199 2200 2201 2202 2203 2204 2205 2206 2207 2208 2209 2210 2211 2212 2213 2214 2215 2216 2217 2218 2219 2220 2221 2222 2223 2224 2225 2226 2227 2228 2229 2230 2231 2232 2233 2234 2235 2236 2237 2238 2239 2240 2241 2242 2243 2244 2245 2246 2247 2248 2249 2250 2251 2252 2253 2254 2255 2256 2257 2258 2259 2260 2261 2262 2263 2264 2265 2266 2267 2268 2269 2270 2271 2272 2273 2274 2275 2276 2277 2278 2279 2280 2281 2282 2283 2284 2285 2286 2287 2288 2289 2290 2291 2292 2293 2294 2295 2296 2297 2298 2299 2300 2301 2302 2303 2304 2305 2306 2307 2308 2309 2310 2311 2312 2313 2314 2315 2316 2317 2318 2319 2320 2321 2322 2323 2324 2325 2326 2327 2328 2329 2330 2331 2332 2333 2334 2335 2336 2337 2338 2339 2340 2341 2342 2343 2344 2345 2346 2347 2348 2349 2350 2351 2352 2353 2354 2355 2356 2357 2358 2359 2360 2361 2362 2363 2364 2365 2366 2367 2368 2369 2370 2371 2372 2373 2374 2375 2376 2377 2378 2379 2380 2381 2382 2383 2384 2385 2386 2387 2388 2389 2390 2391 2392 2393 2394 2395 2396 2397 2398 2399 2400 2401 2402 2403 2404 2405 2406 2407 2408 2409 2410 2411 2412 2413 2414 2415 2416 2417 2418 2419 2420 2421 2422 2423 2424 2425 2426 2427 2428 2429 2430 2431 2432 2433 2434 2435 2436 2437 2438 2439 2440 2441 2442 2443 2444 2445 2446 2447 2448 2449 2450 2451 2452 2453 2454 2455 2456 2457 2458 2459 2460 2461 2462 2463 2464 2465 2466 2467 2468 2469 2470 2471 2472 2473 2474 2475 2476 2477 2478 2479 2480 2481 2482 2483 2484 2485 2486 2487 2488 2489 2490 2491 2492 2493 2494 2495 2496 2497 2498 2499 2500 2501 2502 2503 2504 2505 2506 2507 2508 2509 2510 2511 2512 2513 2514 2515 2516 2517 2518 2519 2520 2521 2522 2523 2524 2525 2526 2527 2528 2529 2530 2531 2532 2533 2534 2535 2536 2537 2538 2539 2540 2541 2542 2543 2544 2545 2546 2547 2548 2549 2550 2551 2552 2553 2554 2555 2556 2557 2558 2559 2560 2561 2562 2563 2564 2565 2566 2567 2568 2569 2570 2571 2572 2573 2574 2575 2576 2577 2578 2579 2580 2581 2582 2583 2584 2585 2586 2587 2588 2589 2590 2591 2592 2593 2594 2595 2596 2597 2598 2599 2600 2601 2602 2603 2604 2605 2606 2607 2608 2609 2610 2611 2612 2613 2614 2615 2616 2617 2618 2619 2620 2621 2622 2623 2624 2625 2626 2627 2628 2629 2630 2631 2632 2633 2634 2635 2636 2637 2638 2639 2640 2641 2642 2643 2644 2645 2646 2647 2648 2649 2650 2651 2652 2653 2654 2655 2656 2657 2658 2659 2660 2661 2662 2663 2664 2665 2666 2667 2668 2669 2670 2671 2672 2673 2674 2675 2676 2677 2678 2679 2680 2681 2682 2683 2684 2685 2686 2687 2688 2689 2690 2691 2692 2693 2694 2695 2696 2697 2698 2699 2700 2701 2702 2703 2704 2705 2706 2707 2708 2709 2710 2711 2712 2713 2714 2715 2716 2717 2718 2719 2720 2721 2722 2723 2724 2725 2726 2727 2728 2729 2730 2731 2

TABLE OF CONTENTS

	<u>Page</u>
ABSTRACT.....	1
1.0 INTRODUCTION.....	2
2.0 EXPERIMENTAL APPROACH.....	4
2.1 Electrochemical Measurements.....	4
2.1.1 Potentiodynamic Polarization Behavior.....	4
2.1.2 AC Impedance Measurements.....	4
2.2 Stress Corrosion Cracking Studies.....	4
3.0 EXPERIMENTAL RESULTS.....	5
3.1 Anodic Polarization Behavior.....	5
3.1.1 Phosphate Solutions.....	5
3.1.2 Carbonate Solutions.....	9
3.1.3 Al 7075 in 1 M NaCl.....	13
3.2 Impedance Spectra.....	13
3.2.1 Steel in Carbonate Solutions.....	13
3.2.2 SS430 in 1 N H ₂ SO ₄	19
3.2.3 Steel in Phosphate Solutions.....	22
3.2.4 Al 7075 in 1 M NaCl.....	25
3.3 CERT - Results.....	29
3.3.1 Phosphate Solutions.....	29
3.3.2 Carbonate Solutions.....	34
4.0 DISCUSSION.....	38
5.0 RECOMMENDATIONS FOR FUTURE WORK.....	46
REFERENCES.....	47

LIST OF TABLES

<u>Table</u>	<u>Page</u>
I Impedance Parameters for C1117 Steel in 1 N NaHCO_3 /0.1 N Na_2CO_3	19
II A.C. Impedance Parameters for 430 SS in 1 N H_2SO_4	22
III A.C. Impedance Parameters for C1117 Steel in 1 N Na_3PO_4 , pH = 4.....	25
IV A.C. Impedance Parameters for Al 7075 in 1 M NaCl.....	27
V Results of Constant Extension Rate Testing.....	31

LIST OF ILLUSTRATIONS

<u>Figure</u>	<u>Page</u>
1 Experimental arrangement for recording of (a) potentiodynamic polarization curves with automatic compensation of the ohmic drop, (b) ac impedance data and (c) CERT with continuous recording of the ac impedance.....	5
2 Anodic potentiodynamic polarization curves for 1008 steel in 1N Na_3PO_4 (pH = 4, 21°C) at three scan rates, uncompensated.....	8
3 Anodic potentiodynamic polarization curves for C1117 steel in 1N Na_3PO_4 (pH = 4, 21°C) at two scan rates with and without compensation of the ohmic drop.....	10
4 Anodic potentiodynamic polarization curves for C1117 steel in 1N Na_3PO_4 , 1N Na_2HPO_4 and 1N NaH_2PO_4 (all at pH = 4, 21°C) at (a) 5 mV/s and (b) 0.2 mV/s, uncompensated.....	11
5 Potentiodynamic polarization curves for 4340 steel in 1N NaHCO_3 /0.1 N Na_2CO_3 , deaerated, at 70°C at three different scan rates for stagnant and rotating electrodes.....	12
6 Potentiodynamic polarization curves for Al 7075 (RCE) in 1 M NaCl (neutral and pH = 12).....	14

LIST OF ILLUSTRATIONS

<u>Figure</u>		<u>Page</u>
7	Complex plane impedance plot (high frequency portion) for 4340 steel in 1N NaHCO ₃ /0.1 Na ₂ CO ₃ , 70°C at three potentials.....	15
8	Complex plane impedance plots for iron (RCE) at three potentials in the active region in 1N NaHCO ₃ /0.1 N Na ₂ CO ₃ , T = 70°C.....	17
9	Complex plane impedance plot for C1117 steel at four potentials in 1N NaHCO ₃ /0.1 N Na ₂ CO ₃ , T = 70°C.....	18
10	Steady state polarization curve for SS 430 (A = 4.0 cm ²) in 1N H ₂ SO ₄ , deaerated, T = 21°C.....	20
11	Impedance plots for SS 430 in 1N H ₂ SO ₄ at potentials as indicated in Fig. 10.....	21
12	Bode-plots for C1117 steel in 1N Na ₃ PO ₄ , pH = 4, T = 21°C as a function of potential.....	23
13	Complex plane plot of high frequency region for C1117 steel in 1N Na ₃ PO ₄ , pH = 4, T = 21°C at E = 0 mV.....	24
14	Bode-plots for Al 7075-T6 (RCE) in neutral 1M NaCl, T = 21°C as a function of potential.....	26
15	Bode-plots for Al 7075-T6 (RCE) in 1M NaCl, pH =12 as a function of potential.....	28
16	Typical stress/strain curves for C1117 in 1N Na ₃ PO ₄ and in mineral oil.....	30
17	Relative reduction in area (RA) for C1117 steel in 1N Na ₃ PO ₄ , pH = 4.....	32
18	Relative RA for C1117 steel in carbonate/bicarbonate solution.....	33
19	Bode plots for C1117 steel in 1N Na ₃ PO ₄ , pH = 4, under elastic strain at -400, 0, 100 and 400 mV.....	35
20	Phase angle changes resulting from straining C1117 steel in 1N Na ₃ PO ₄ at 0 mV.....	36

LIST OF ILLUSTRATIONS

<u>Figure</u>		<u>Page</u>
21	Bode plots for C1117 steel in 1 N Na_2CO_3 /0.1 N NaHCO_3 at 70°C under elastic strain.....	37
22	Phase angle plots for C1117 steel in 1N Na_2CO_3 /0.1 N NaHCO_3 at -690 mV at different strains.....	39
23	Phase angle plots for C1117 steel in 1N Na_2CO_3 /0.1 N NaHCO_3 at -750 mV at different strains.....	40
24	Model for impedance of C-Mn steel. Circuit analogs of surface films.....	43
25	Model for impedance of C-Mn steel. Schematic Bode plots for cases presented in Fig. 24.....	44

ABSTRACT

Electrochemical techniques for predicting stress corrosion cracking (SCC) susceptibility have been evaluated and constant extension rate tests (CERT) have been performed for a C-Mn Steel (C1117) in 1 M Na_3PO_4 , pH = 4, $T = 21^\circ\text{C}$ and in 1.0 M $\text{NaHCO}_3/0.1 \text{ M Na}_2\text{CO}_3$, $T = 70^\circ\text{C}$ at controlled potentials with continuous recording of the a.c. impedance in a frequency range between 10 KHz and 30 mHz. These tests have been carried out in potential regions of susceptibility to SCC which were determined by comparing fast and slow anodic potentiodynamic polarization curves as suggested by Parkins and by analysis of a.c. impedance data as suggested by Armstrong. The occurrence of a high frequency relaxation phenomenon at the potential region where maximum susceptibility to SCC is observed seems to indicate that impedance spectra can be used to assess the SCC behavior. A model for the changes in surface structure occurring during CERT and the resulting impedance behavior is discussed.

1.0 INTRODUCTION

This report summarizes the results obtained in a project in which electrochemical and mechanical impedance techniques were applied to the evaluation of environmental cracking of steels and aluminum alloys. Electrochemical impedance measurements are finding increased application in studies of electrode kinetics, passivation phenomena and corrosion inhibition by organic and inorganic compounds and by polymer coatings. The mechanical impedance of an oxide layer has only recently been studied by a group in Belgium.⁽¹⁾ This method assumes a correlation between mechanical stress and the electrochemical response of the material.

Since environmentally induced failure by stress corrosion cracking (SCC) and corrosion fatigue (CF) can be assumed to involve electrochemical processes, it has been recognized that it is very important to carry out SCC and CF tests under precise control of the electrochemical conditions. However, very few attempts have been made to apply more sophisticated techniques such as impedance measurements to monitoring of the events which occur during the cracking process. At present constant extension rate tests (CERT) are being performed as a function of potential without monitoring of the electrochemical response of the system to the applied stress. The approach taken in this laboratory tries to fill this gap by monitoring the electrochemical and mechanical impedance response during SCC and CF tests, and to use the resulting information to obtain a detailed mechanistic understanding of these failure phenomena. Based on this information, it should be possible to develop the impedance technique as a test method for determining the susceptibility of structural materials to SCC and CF, and use the technique as a criterion for material selection.

Several approaches reported in the literature for using electrochemical techniques to determine the potential regions where steels are susceptible to SCC have been evaluated in this project. Parkins' criterion⁽²⁾ is based on the different passivation behavior in the active-to-passive transition region for potentiodynamic polarization curve recorded at slow and fast scan rates. Large differences in the passivation current are assumed to indicate susceptibility to SCC because the metal surface is not able to follow fast changes in external

passivation conditions. SCC requires a critical balance between active dissolution and repassivation. Armstrong, et al.⁽³⁾ have made measurements of relaxation times for passivation by means of the a.c. impedance techniques and have established empirical correlations to the known SCC susceptibility for low carbon steel in carbonate/bicarbonate solutions at 70°C.

Anodic potentiodynamic polarization curves have been obtained for a C-Mn steel in 1 M Na_3PO_4 , pH =4 and in a carbonate/bicarbonate solution and a.c. impedance measurements have been made in the different characteristic portions of these polarization curves. A few such experiments have also been carried out for iron and a high strength steel and for Al 7075.

Equipment for CERT has been assembled and tests have been carried out for a C-Mn steel in phosphate and in carbonate/bicarbonate solutions at controlled potential with continuous monitoring of the impedance behavior in a wide frequency range (10 kHz - 30 MHz). The data have been analyzed in terms of the type and number of relaxation times observed in different regions of the stress-strain curve and comparisons have been made with the results based on Parkins' criterion and the impedance behavior of the unstressed materials.

2.0 EXPERIMENTAL APPROACH

2.1 Electrochemical Measurements

2.1.1 Potentiodynamic Polarization Behavior

Potentiodynamic polarization curves have been obtained for stagnant electrodes and for rotating cylinder electrodes (RCE)⁽⁴⁾ using a PAR potentiostat 173 with a sweep generator 175. The RCEs were used to provide controlled mass transport conditions. The sweep rates were between 0.2 mV/s and 50 mV/s according to Parkins.⁽²⁾

Since the critical current density for passivation is fairly high ($> 100 \text{ mA/cm}^2$) for all solutions which were selected to study the impedance and SCC of steel, it is necessary to compensate the ohmic drop between the Luggin capillary and the sample surface. This becomes especially important in the application of Parkins' criterion in which a narrow potential region of SCC susceptibility is to be detected. Automatic compensation of the ohmic drop has been achieved using the interruptor unit PU1⁽⁵⁾ connected to the potentiostat as described elsewhere.⁽⁶⁾ Figure 1a shows the experimental arrangement.

2.1.2 A.C. Impedance Measurements

The a.c. impedance measurements were performed using the automated system described elsewhere⁽⁷⁾ which consists of a Solartron 1174 Transfer Function Analyzer (TFA), a Hewlett Packard computer 9825S and a HP plotter 9872B (Fig. 1b). The impedance measurements were usually carried out over a frequency range of 100 KHz to 25 MHz with 10 frequencies per second and 10 cycles per frequency. The impedance was determined at controlled potential for unstressed samples or for stressed samples during the CERT.

2.2 Stress Corrosion Cracking Studies

The susceptibility to SCC was determined in CERT at controlled potential with continuous recording of the a.c. impedance. Figure 1c shows the schematic of the combined CERT equipment and a.c. impedance monitoring system.

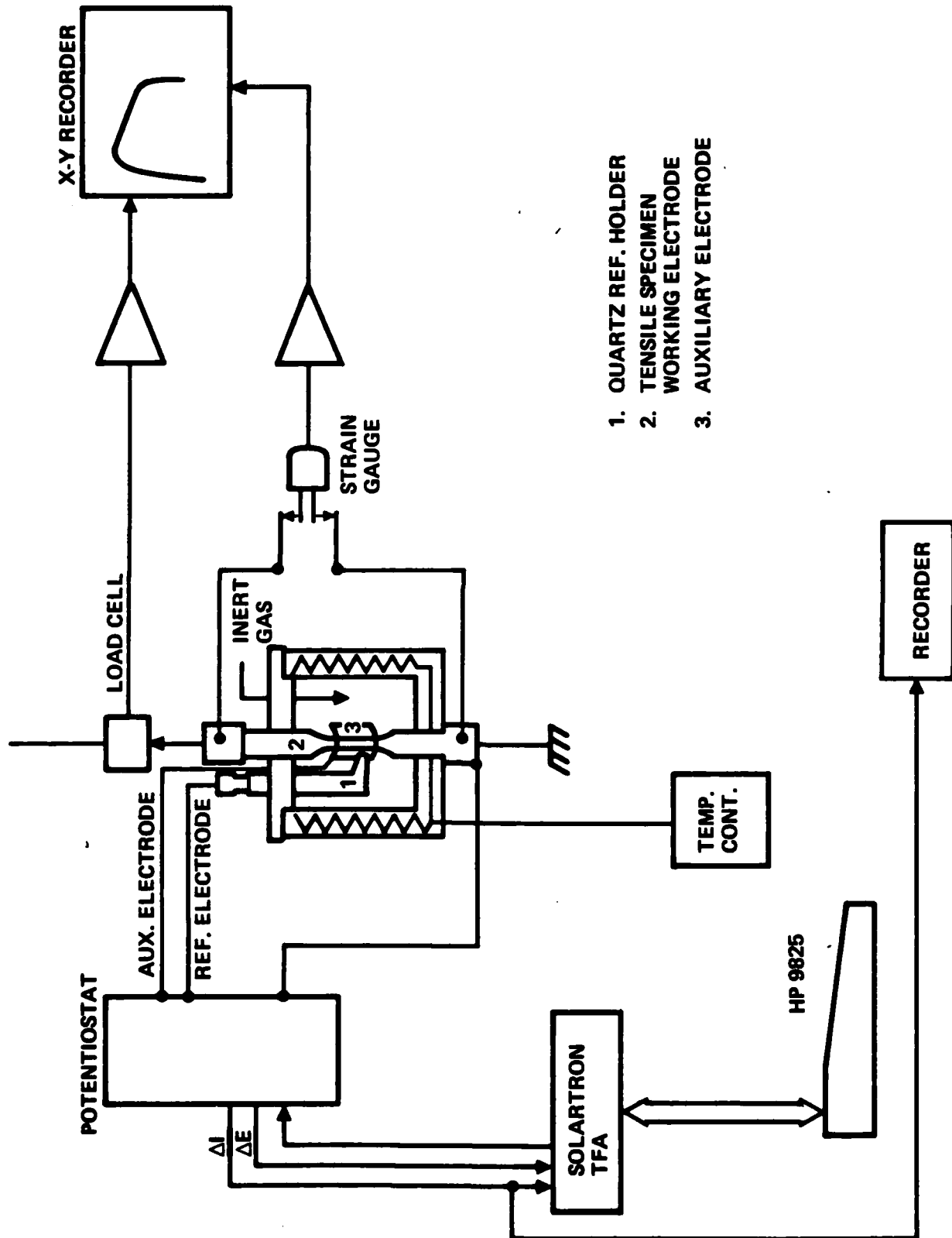


Fig. 1 Experimental arrangement for recording of (a) potentiodynamic polarization curves with automatic compensation of the ohmic drop, (b) ac impedance data and (c) CERT with continuous recording of the ac impedance.

A constant drive system (W.T. Specialty Co., P-2000) including a variable speed motor with appropriate variable-ratio reduction gears, BLH 2000 lb capacity load cell and test frame comprise the mechanical component of the CERT machine. The output of the load cell and strain gauge (Fig. 1c) are amplified with Gould bridge amplifiers which drive the respective Y and X channels of an X-Y recorder. The low load alarm of the local cell amplifier activates a latching relay which disconnects power to the potentiostat and motor when the specimen breaks. The specimens are 0.25 in. (0.635 cm) diameter "dog-bone" tensile specimens which have a gauge length of 0.5 in. (1.27 cm) and gauge diameter of 1/8 in. (0.32 cm). The tensile samples were masked with an epoxy coating so as to expose only the reduced gauge length. Since Parkins observed little difference in the SCC behavior of cold worked or annealed C-Mn steel in phosphate solutions,⁽⁹⁾ tests were performed using as-received specimens. The typical chemical composition (AISI) of C1117 steel is 0.14 - 0.20% C, 1.00 - 1.30% Mn, 0.040 % max P, 0.08 - 0.13% S. The cross head speed was set to $1.25 \cdot 10^{-6}$ in./s in order to give the $2.5 \cdot 10^{-6} s^{-1}$ strain rate used by Parkins et al.^(8,9)

A 12.5 diameter by 11 cm deep teflon container held the electrolytes of 1 N $NaCO_3$ /0.1 N $NaHCO_3$ or 1 M Na_3PO_4 adjusted to pH 4 with H_3PO_4 . Teflon fittings in the top and the bottom of the container provided a water-tight seal about both ends of the specimen. The teflon lid of the container held the quartz reference electrode compartment, a polyethylene inert gas purging line, leads to the wire gauge Pt-auxiliary electrode, thermister probe for the temperature controller, and a thermometer with a stainless steel body. The quartz reference electrode compartment held a saturated calomel reference electrode (SCE). The compartment formed a Luggin capillary extending to within about 1 cm of the gauge section. A Pt auxiliary electrode surrounded the gauge section of the tensile specimen. The walls of the teflon container held heating elements powered by the proportional controller. A controlled potential was maintained throughout the CERT using the potentiostat and the a.c. impedance was determined continuously as described above. While most CERT were conducted in the regions of SCC susceptibility which were estimated from potentiodynamic polarization curves, some CERT were run also outside that region for control purposes.

3.0 EXPERIMENTAL RESULTS

3.1 Anodic Polarization Behavior

Potentiodynamic polarization curves have been initially obtained for iron, 4340 steel, C1117 C-Mn steel and stainless steel type 430 in 0.1 M Na_2SO_4 with or without $\text{Na}_2\text{Cr}_2\text{O}_7$ at 21°C, in 1.0 M NaNO_3 at 21°C and in 1.0N H_2SO_4 at 21°C as discussed in Progress Report No.1. Further studies have concentrated on 1.0 M Na_3PO_4 (pH = 4) at 21°C and 1.0 M NaHCO_3 /0.1 M Na_2CO_3 at 70°C since Parkins et al^(8,9) had reported polarization and CERT data in these solutions for a C-Mn steel. Polarization curves have also been recorded for Al 7075-T6 in 1 M NaCl at pH = 7 and 12.

3.1.1 Phosphate Solutions

An interesting situation exists for the phosphate solutions since Parkins et al⁽⁹⁾ report that SCC occurred in 1 M Na_3PO_4 and in 1 M Na_2HPO_4 , but not in 1 M NaH_2PO_4 (all solutions adjusted to pH = 4). Since it is unlikely that these three solutions at pH = 4 can produce drastically different corrosion behavior, a comparison of the anodic polarization curves in these media was made.

Figure 2 shows an anodic potentiodynamic polarization curve for 1008 steel in 1 M Na_3PO_4 (pH = 4, 21°C) at three different scan rates between 0.5 mV/s and 10 mV/s. While identical behavior is observed in the active region, a large dependence on scan rate is found for the active-to-passive transition region and the passive region. Parkins^(2,8,9) determines the region of SCC susceptibility by taking the ratio of the current for the fast and the slow scan rate. If this ratio exceeds 1000, it is assumed that SCC will occur in this potential region. Since for the example in Fig. 2, a ratio of 1000 was never exceeded, a ratio of 100 was used. Based on this criterion SCC is predicted between + 60 mV and +330 mV vs SCE, if the scans obtained with 0.5 and 2 mV/s are compared, and between +50 mV and + 555 mV, if the scans 0.5 and 10 mV/s are used. This result shows some weakness in this approach since the prediction depends on the scan rates used in the test. Another problem is due to the uncompensated ohmic resistance.

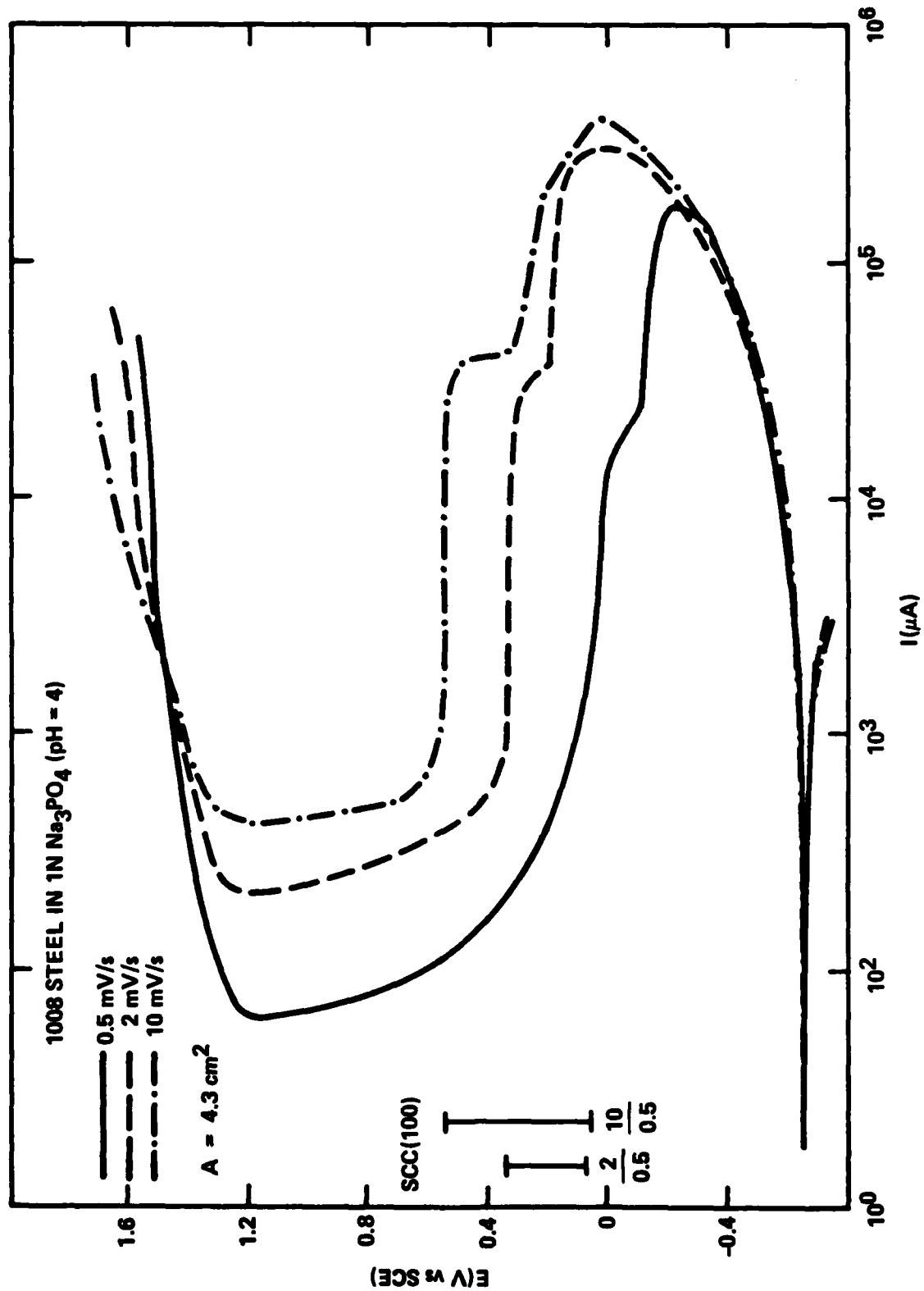


Fig. 2 Anodic potentiodynamic polarization curves for 1008 steel in 1N Na_3PO_4 (pH = 4, 21°C) at three scan rates, uncompensated.

Despite the good conductivity of the test solution, the ohmic drop can reach a few hundred mV for a critical current density, i_{crit} , of 100 mA/cm^2 , especially if surface layers are formed in the active dissolution region. Figure 3 gives an example for polarization curves with and without automatic compensation of the ohmic drop (Fig. 1a) at two scan rates. For the fast scan rate (5 mV/s) the true critical potential for passivation E_{crit} is about 400 mV more negative when the ohmic drop is eliminated. For the slower scan rate (0.2 mV/s) the difference in E_{crit} is smaller due to the smaller i_{crit} . The difference in i_{crit} for the two scan rates is due to another error as a result of uncompensated ohmic drop. Only for a potentiodynamic polarization curve free of ohmic drop is the scan rate seen by the working electrode constant. Without compensation the scan rate is dependent on the ohmic drop and therefore on the potential.

The region of SCC is estimated to be between 0 mV and + 250 mV based on the uncompensated curves and between + 50 mV and + 200 mV for the compensated curve (Fig. 3). For the same system Parkins et al.⁽⁹⁾ estimates a cracking range between - 100 mV and -470 mV.

The claim by Parkins et al.⁽⁹⁾ that steel cracks in 1 M Na_3PO_4 and in 1 M Na_2HPO_4 , but not in 1 M NaH_2PO_4 (all at $\text{pH} = 4$) was checked by running potentiodynamic polarization curves for C-Mn steel C1117 in these solutions (Figs. 4a and b). Although there are some differences in passivation behavior, an active-to-passive transition is found for all three solutions as expected. By comparing the current flow for fast and slow scans, the regions of susceptibility to SCC are estimated as shown in Fig. 4a.

3.1.2 Carbonate Solutions

The polarization curves in 1 M NaHCO_3 /0.1 M Na_2CO_3 at 70°C , deaerated are shown for 4340 steel in Fig. 5. Similar results were obtained for C1117 and for iron. Experiments were carried out at three scan rates (0.5 mV/s , 20 mV/s , and 50 mV/s) for stagnant and rotating ($\omega = 144 \text{ rad/s}$) electrodes. Based on the polarization curves in Fig. 5 and a ratio of 100 for susceptibility to SCC the steel should not crack at all; a factor of above 70 is found between -200 mV and

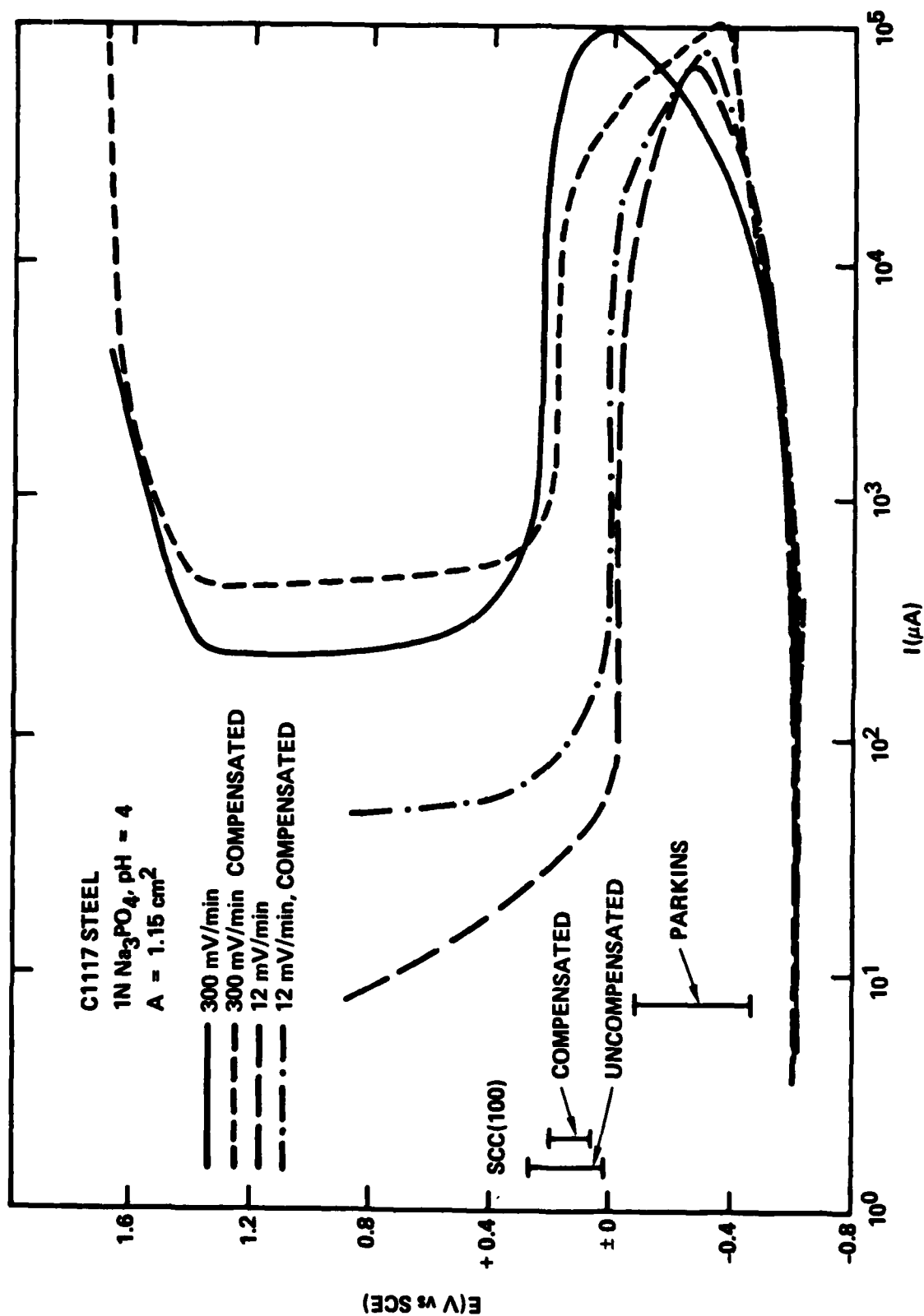


Fig. 3 Anodic potentiodynamic polarization curves for C1117 steel in 1N Na_3PO_4 (pH = 4, 21°C) at two scan rates with and without compensation of the ohmic drop.

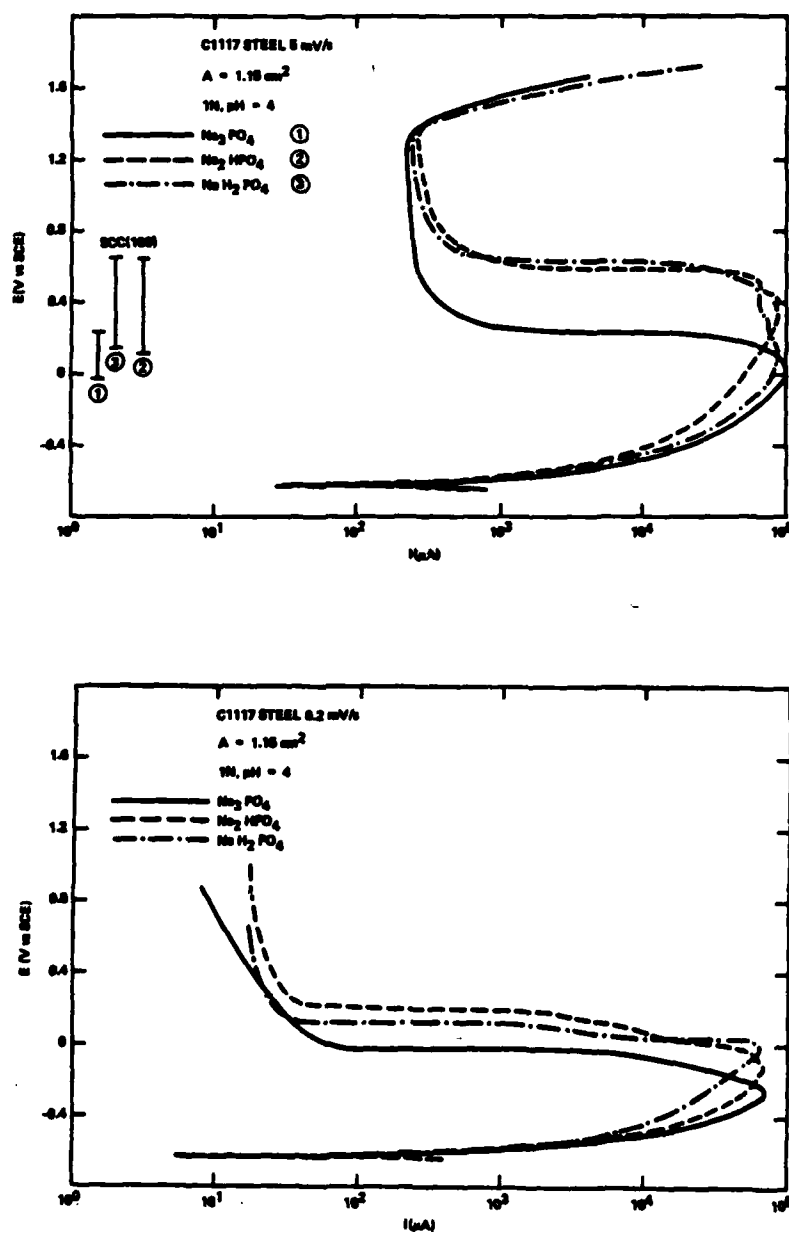


Fig. 4 Anodic potentiodynamic polarization curves for C1117 steel in 1N Na_3PO_4 , 1N Na_2HPO_4 and 1N NaH_2PO_4 (all at pH = 4, 21°C) at (a) 5 mV/s and (b) 0.2 mV/s, uncompensated.

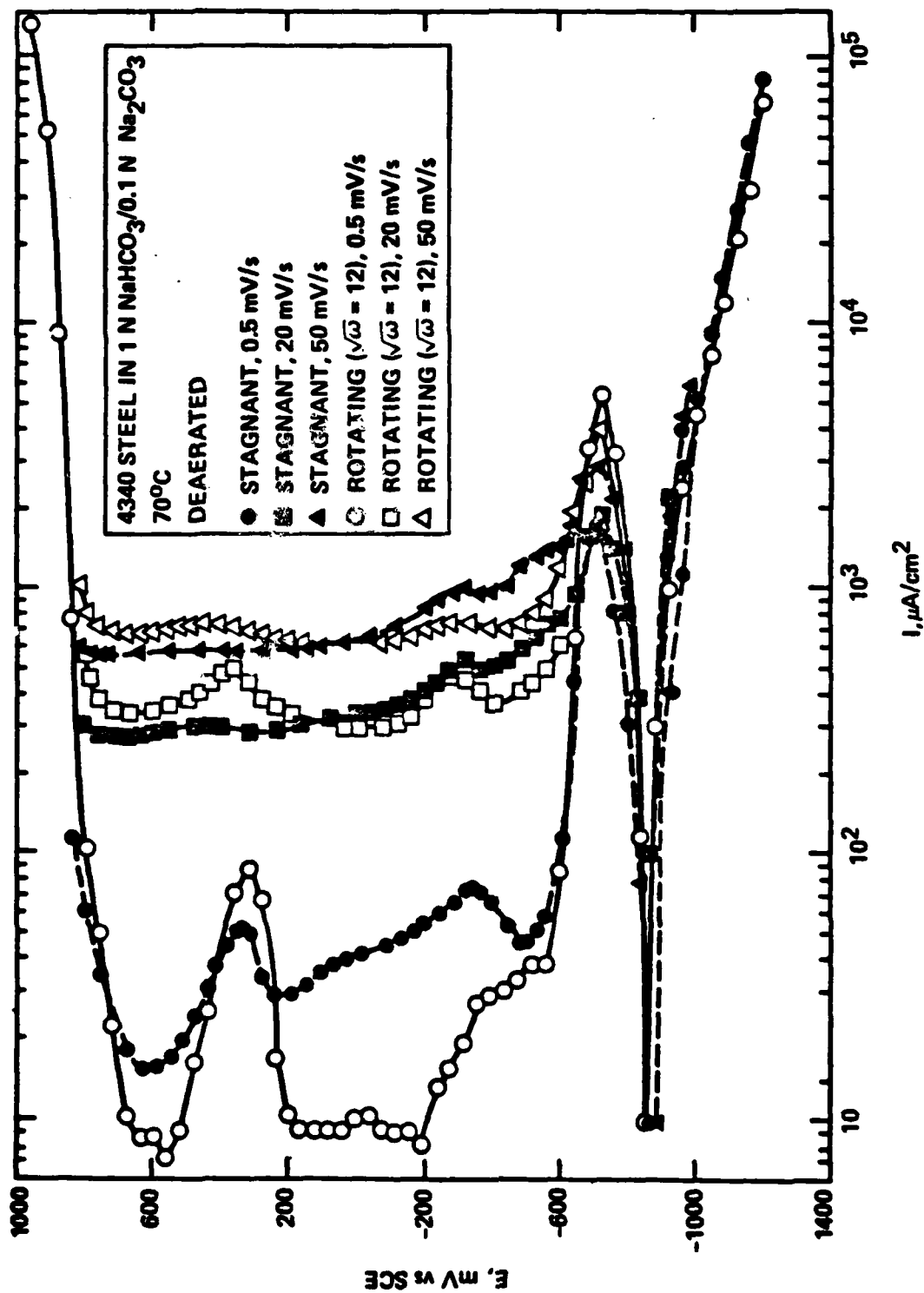


Fig. 5 Potentiodynamic polarization curves for 4340 steel in 1N NaHCO_3 /0.1 N Na_2CO_3 , deaerated, at 70°C at three different scan rates for stagnant and rotating electrodes.

+200 mV. While there are pronounced differences in the passive region for polarization curves obtained at fast and slow scan rates, the current ratio is less than 100. Parkins et al.⁽⁸⁾ found a narrow region for SCC susceptibility between about -675 mV and -575 mV in 1 M Na_2CO_3 + 1 M NaHCO_3 at 70°C based on reduction in area at fracture.

3.1.3 Al 7075 in 1 M NaCl

The potentiodynamic polarization curves for Al 7075-T6 are shown in Fig. 6. Since pitting in neutral 1M NaCl occurs at or close to E_{corr} , the specimen cannot be polarized anodically. In the cathodic branch of the polarization curve, a limiting current for oxygen reduction and the potential region where H_2O -reduction occurs can be seen. At pH = 12 an active-to-passive transition is observed; however, the anodic current is high.

3.2 Impedance Spectra

3.2.1 Carbonate Solutions

The results obtained by Parkins et al.^(8,9) in phosphate and carbonate solutions have suggested that maximum susceptibility to SCC occurs in the active-to-passive transition of the anodic polarization curve. Similarly, Armstrong⁽³⁾ has suggested that the time constant, τ , which has a maximum in the active-to-passive transition, indicates susceptibility to SCC. It was planned, therefore, to concentrate on a.c. impedance measurements in this transition region and to compare the impedance data with the polarization data reported above. However, initial tests in carbonate solutions showed that a fundamental problem exists in the recording of impedance data in the active-to-passive transition regions. A true impedance can be obtained only at steady state conditions over the time period it takes for recording the whole frequency range (about 1 h). However, it was noted that at constant potential the current decreased continuously and finally became cathodic indicating passivation. The resulting typical passive impedance behavior is shown in Fig. 7 as a complex plane plot of the (negative) imaginary part of the impedance Z'' vs the real part Z' . A high frequency relaxation appears as an inflection in the impedance plot

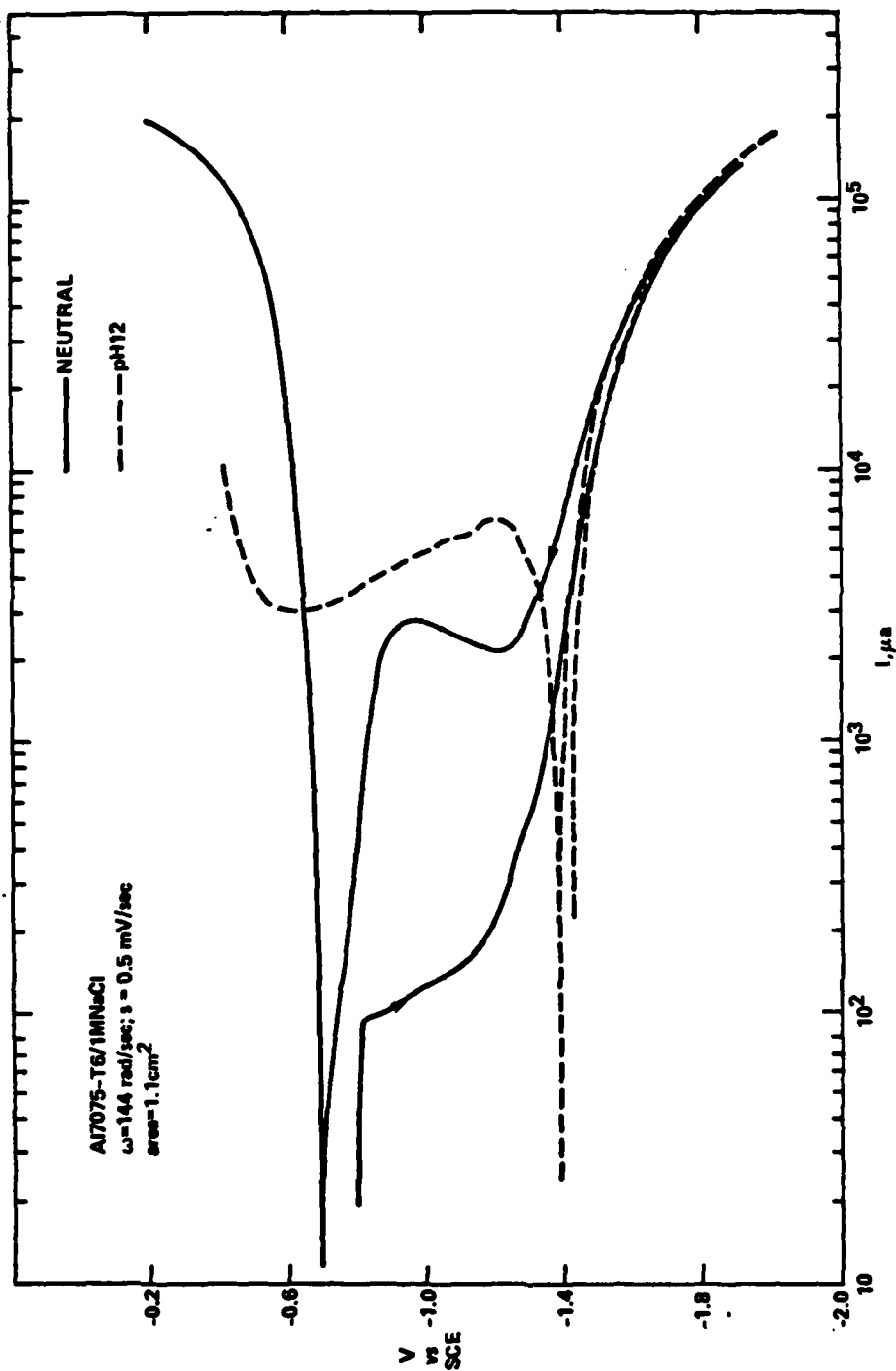


Fig. 6 Potentiodynamic polarization curves for Al 7075 (RCE) in 1 M NaCl (neutral and pH = 12).

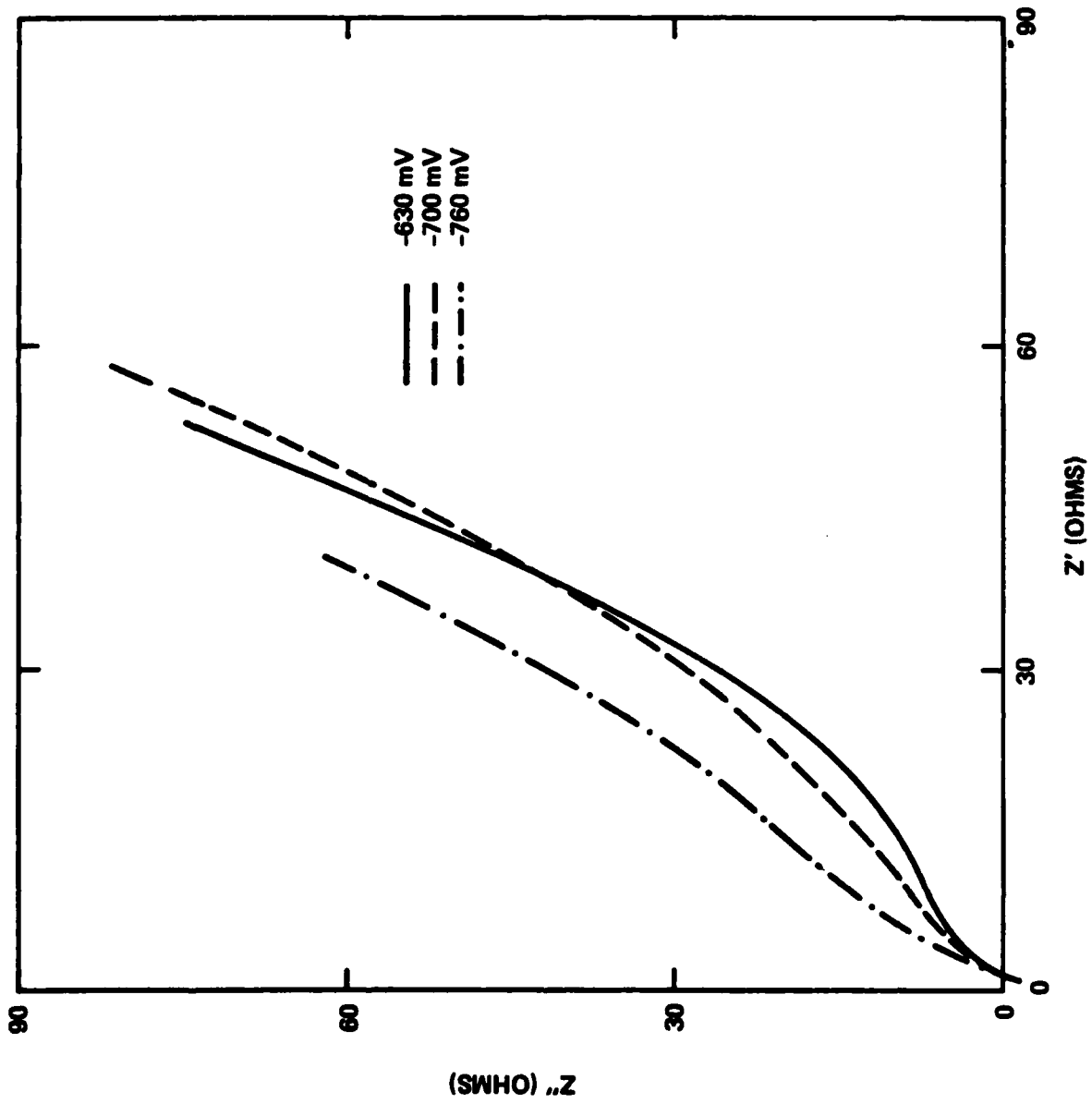


Fig. 7 Complex plane impedance plot (high frequency portion) for 4340 steel in 1N $\text{NaHCO}_3/0.1 \text{ Na}_2\text{CO}_3$, 70°C at three potentials.

which could be due to a reaction in the passive film or at the film/electrolyte interface. If the steel was passivated at $E > -600$ mV and then polarized into the active region, reactivation did not occur and the impedance spectrum was similar to that shown in Fig. 7 at -760 mV. However, when active dissolution occurs in this region of the polarization curve, two more or less well defined semicircles appear as shown in Fig. 8 for an iron RCE.

Since the potential region where a negative slope exists was inaccessible for steady-state impedance measurements, a test was carried out in which a minimum number of frequencies at a minimum measuring time at each frequency was used. Figure 9 is an example of this type of measurement. At -680 mV which is in the active-to-passive transition a "backward going" semicircle occurs with a zero frequency intercept at the negative Z' -axis similar to Armstrong's results.⁽³⁾ A more detailed analysis is given in Table I for a different experiment over a wider potential range. Between -745 mV and -685 mV a very broad semicircle occurred and only the intercept R_1 and the zero frequency limit could be detected. The frequency f_1 corresponds to the maximum of Z'' and is related to the electrode capacitance C by:

$$f_1 = \frac{1}{2\pi R_1 C} \quad (1)$$

Between -685 mV and -625 mV two semicircles appeared which allowed calculation of the time constant, τ , according to Armstrong⁽³⁾ as:

$$\tau = \frac{1}{2\pi f_2} \left(\frac{R_2}{R_2 - R_1} \right) ,$$

where R_1 and R_2 are corrected for the solution resistance R_Ω , which is the high frequency intercept in a complex plane plot. At the transition from the active dissolution to the active-to-passive transition region ($E = -685$ mV to -665 mV), $\tau = 1.84$ s and 1.16 s, respectively, while $\tau = 0.27$ s at $E = -625$ mV. Despite the fact that the impedance measurements were carried out in a minimum time, the current of each applied potential E_{app} changed appreciably and became cathodic in several cases (Table I).

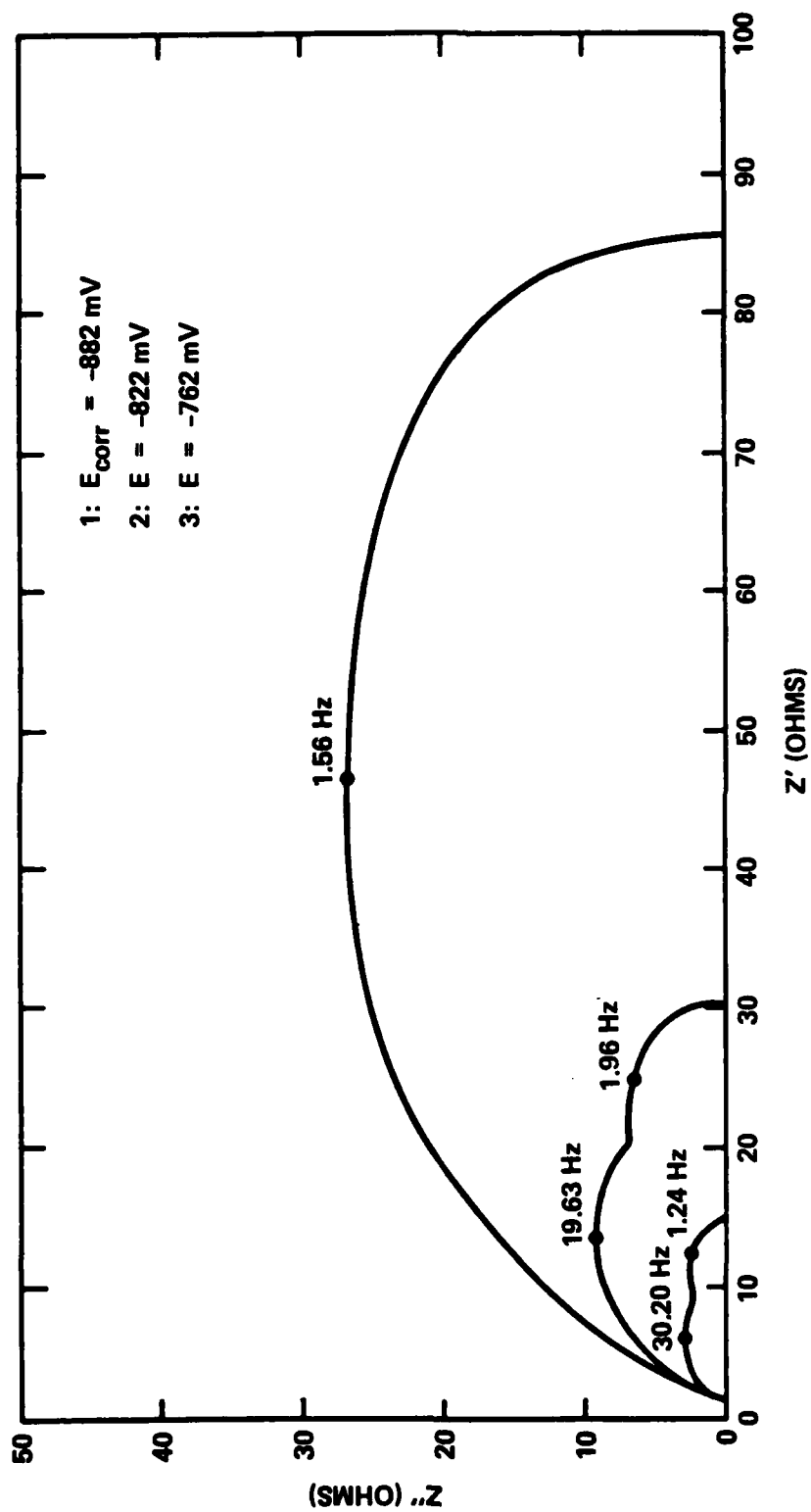


Fig. 8 Complex plane impedance plots for iron (RCE) at three potentials in the active region in 1N $\text{NaHCO}_3/0.1 \text{ N Na}_2\text{CO}_3$, $T = 70^\circ\text{C}$.

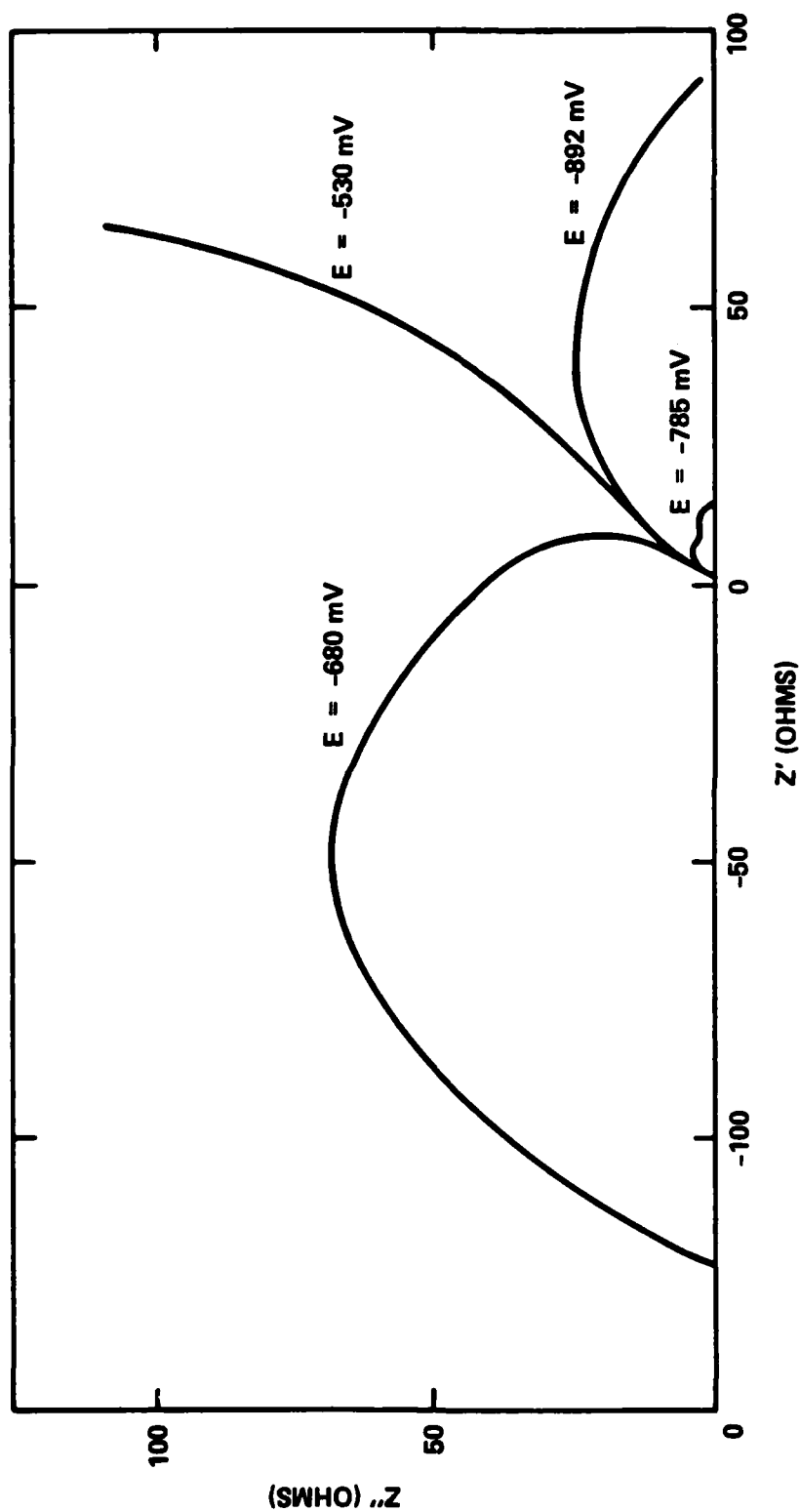


Fig. 9 Complex plane impedance plot for C1117 steel at four potentials in 1N $\text{NaHCO}_3/0.1\text{N}$ Na_2CO_3 , $T = 70^\circ\text{C}$.

Table I
A.C. Impedance Parameters for C1117 Steel in 1 N NaHCO₃/0.1 N Na₂CO₃

E_{app} (mV)	Current		R_1 (Ω)	R_2 (Ω)	f_1 (Hz)	f_2 (Hz)	τ (s)
	(μ A) Initial	(μ A) Final					
-745	110	-10	280	n.d.	2.5	n.d.	
-725	30	2	440	n.d.	2.5	n.d.	
-695	2350	250	125	n.d.	1.0	n.d.	
-685	2700	1000	17	26	25	0.25	1.84
-665	740	-140	32	102	1.6	0.2	1.16
-625	-230	-200	1000	-110	1.6	0.06	0.27
-605	-240	-240	100	$\rightarrow \infty$	0.6	<0.03	

n.d.: not determined.

3.2.2 SS430 in 1N H₂SO₄

A system which exhibits a stable active-to-passive transition is type 430 stainless steel in 1 N H₂SO₄. Figure 10 shows the anodic polarization curve and Figs. 11a and b the impedance plots. At the corrosion potential, E_{corr} , and at a potential in the active region (point 2 in Fig. 10) the impedance plots are approximate semicircles. At -400 mV a second relaxation phenomenon appears as an additional semicircle with the low frequency intercept at negative Z' -values (Fig. 11a, curve 3). Similar behavior is found at -327 mV and at -300 mV as predicted for the active-to-passive transition (points 4 and 5 in Fig. 10). At +63 mV which is in the passive region (point 6 in Fig. 10) the impedance again attains values only in the first quadrant of the complex plane, but remains predominantly capacitive as is characteristic for the passive state. Table II gives an analysis for the six potentials where the impedance was measured. The time constant, τ , was calculated according to Eq. (1).

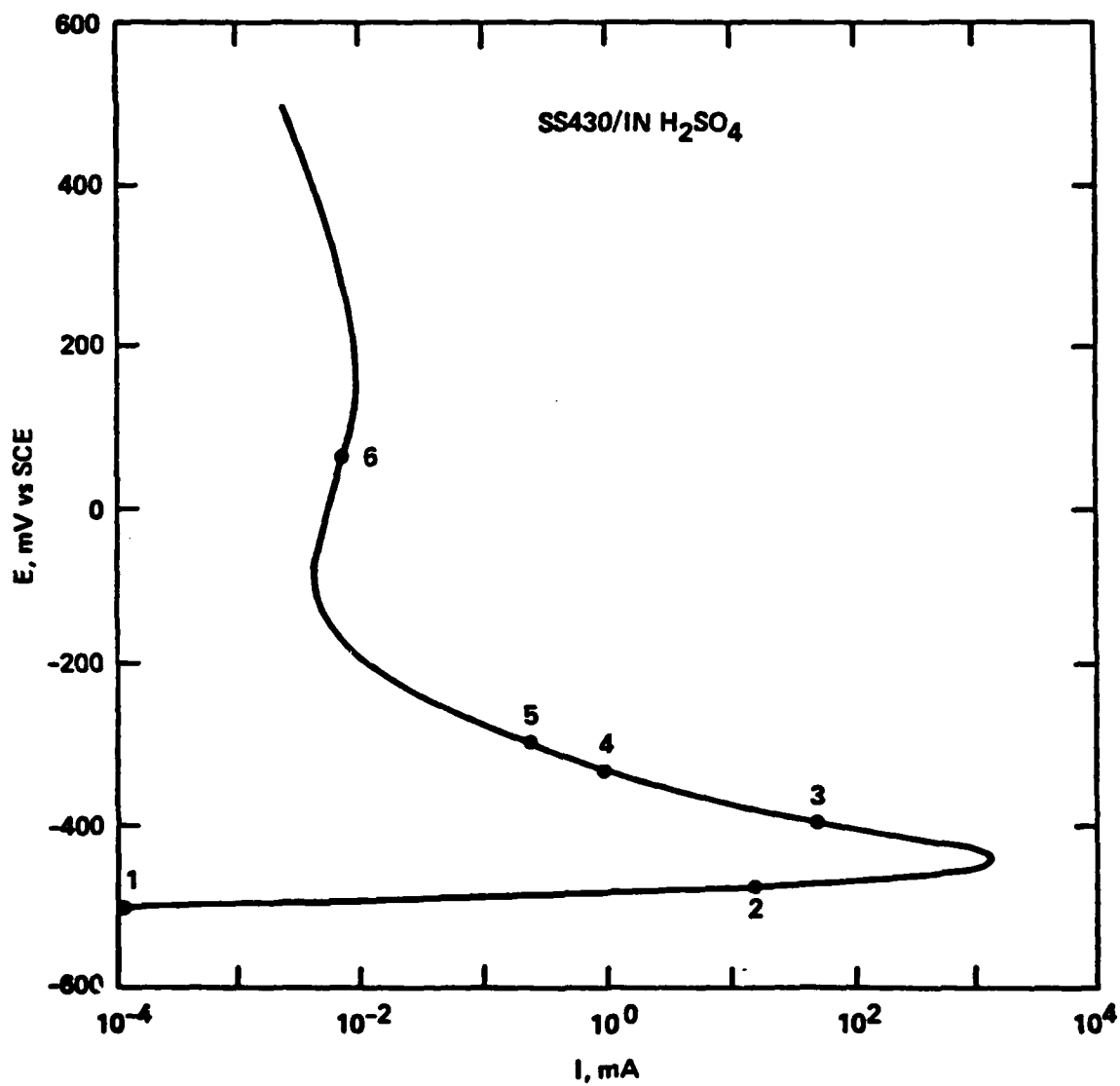


Fig. 10 Steady state polarization curve for SS 430 ($A = 4.0 \text{ cm}^2$) in 1N H₂SO₄, deaerated, $T = 21^\circ\text{C}$.

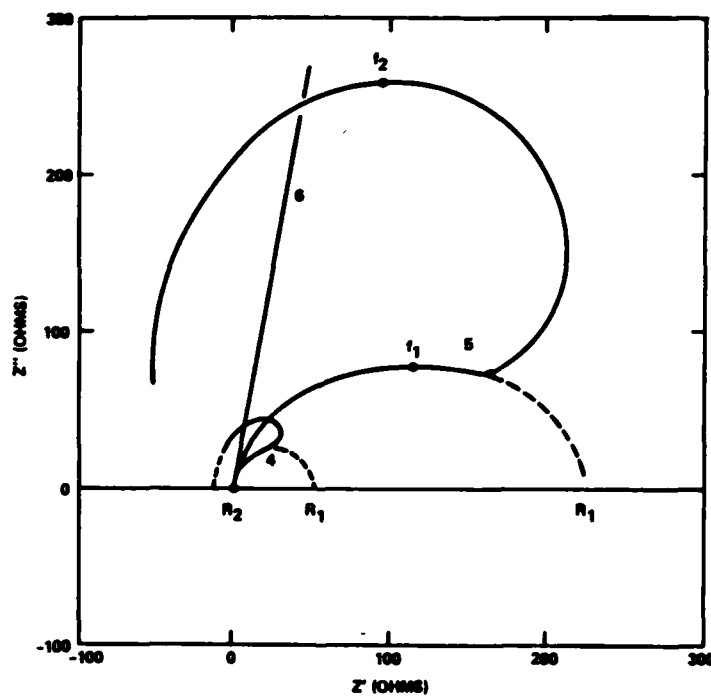
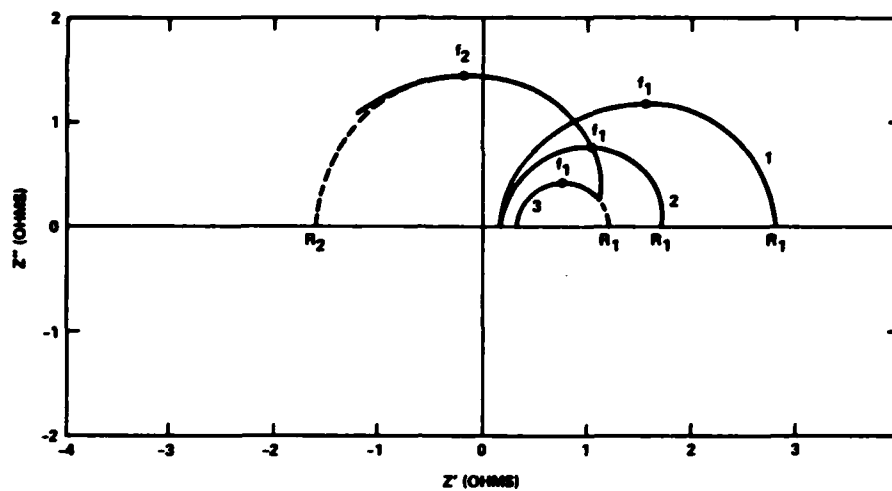


Fig. 11 Impedance plots for SS 430 in 1N H_2SO_4 at potentials as indicated in Fig. 10.

Table II
A.C. Impedance Parameters for 430 SS in 1 N H₂SO₄

E (mV)	I (mA)	R ₁ [*] (Ω)	R ₂ [*] (Ω)	f ₁ (Hz)	f ₂ (Hz)	τ (s)
-513	0	1.4	n.d.	49	n.d.	
-476	15.6	2.5	n.d.	63	n.d.	
-400	47.0	0.80	-1.4	49	0.39	0.26
-327	0.88	~ 60	-11.0	0.4	0.1	0.25
-300	0.25	220	<-56	1.0	0.015	~ 2.15
+63	0.0073	∞				

*Corrected for solution resistance R_s.

3.2.3 Steel in Phosphate Solutions

The impedance behavior of C1117 steel in 1 M Na₃PO₄, pH = 4 is shown in Fig. 12 as Bode-plots (log |Z| vs log ω) for E_{corr} and potentials in the active (E = -400 mV), active-to-passive (E = 0 mV) and passive region (E = +540 mV, +1000 mV). Table III gives an analysis of these data. At = -640 mV = E_{corr}, -400 mV and +1000 mV one depressed semicircle with its center below the Z'-axis was found. At +540 mV capacitive behavior is observed which is typical of the passive state. At E = 0 mV a high frequency relaxation exists and capacitive behavior occurs at lower frequencies. The high frequency behavior as shown in Fig. 13 appeared at potential where failure occurred in the CERT as will be discussed below. An interesting result of Table III is the increase of R_Ω in the passive region from values which could be attributed to the electrolyte resistance to values which are 3 to 4 times as high. Apparently salt or corrosion product layers are formed.

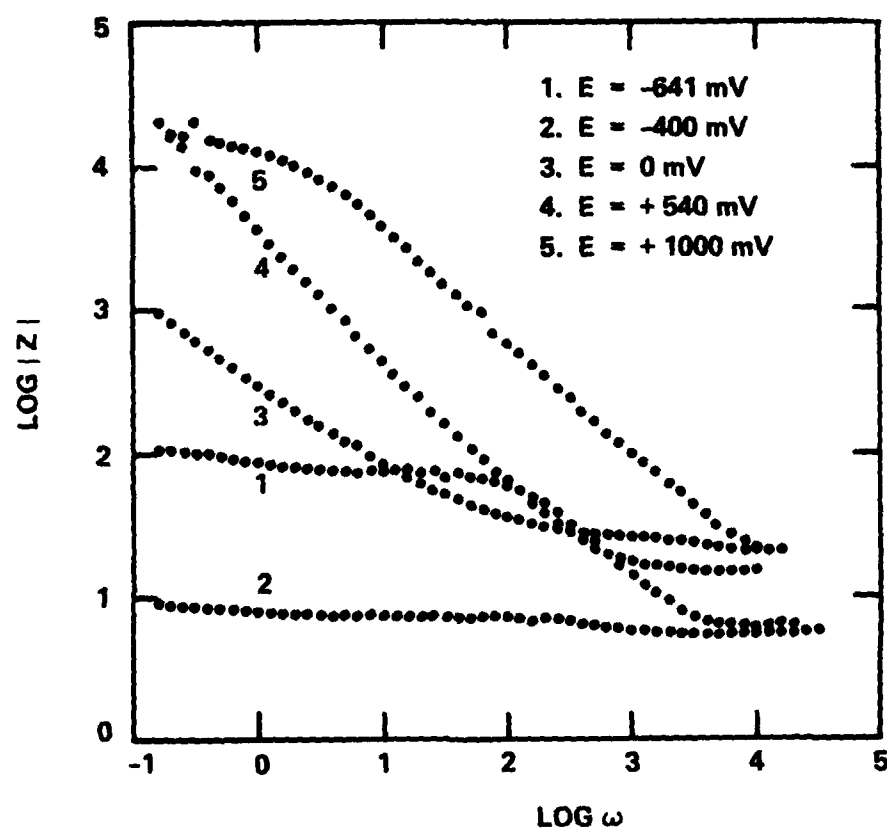


Fig. 12 Bode-plots for C1117 steel in 1N Na_3PO_4 , $\text{pH} = 4$, $T = 21^\circ\text{C}$ as a function of potential.

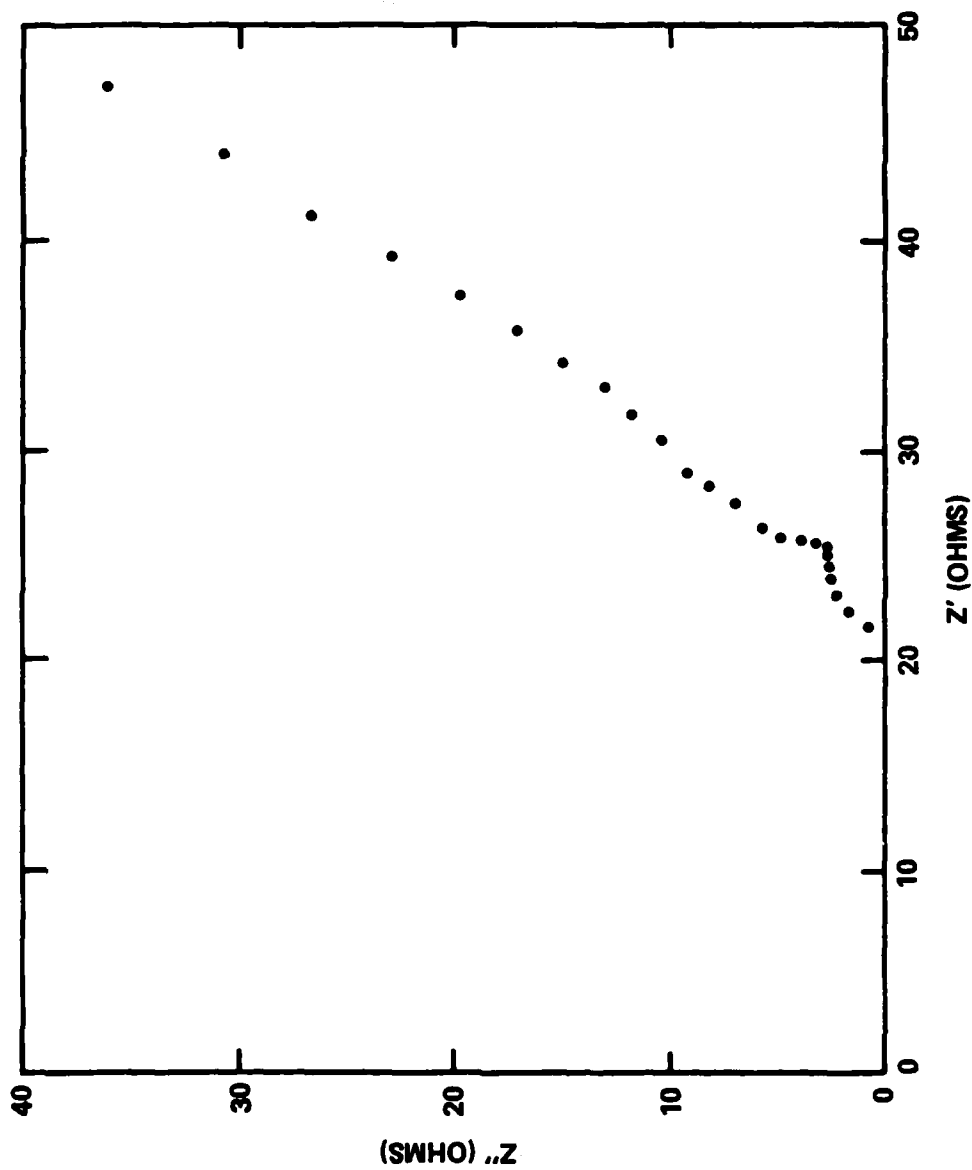


Fig. 13 Complex plane plot of high frequency region for C1117 steel in 1N Na_3PO_4 , pH = 4, T = 21°C at E = 0 mV.

Table III
A.C. Impedance Parameters for C1117 Steel in 1 N Na_3PO_4 , pH = 4

E (mV vs SCE)	$I_{d.c.}$ (mA)	R_2 (ohm)	R_p (ohm)	C (μF)	DC Behavior
-640	0	6	71	90	E_{corr}
-400	25-21	5	2	n.d.	Active
± 0	0.004-0.002 [†]	21	>1000	85	Active-Passive
+540	0.003-0.002	15	>3 $\cdot 10^4$	300	Passive
+1000	0.011-0.005	22	14300	30	Passive

[†]Indicates change of $I_{d.c.}$ during experiment.

3.2.4 Al 7075 in 1M NaCl

Since pitting occurs upon anodic polarization of Al 7075 in neutral 1 M NaCl, impedance data have only been obtained at cathodic potentials as shown in Fig. 14. At E_{corr} corrosion rates are very low and predominantly capacitive behavior occurs in the frequency range studied. At $E = -1220$ mV and -1280 mV in the limiting current region the impedance levels off at lower frequencies and a zero frequency limit R_2 can be given as shown in Table IV. At $E = -1440$ mV, which is in the H_2O reduction region, two time constants seem to occur, but the data are difficult to analyze.

At pH = 12 impedance data (Fig. 15) were taken in the anodic region (see Fig. 6). At $E_{\text{corr}} = -1400$ mV complex plane analysis shows a broad semicircle which is difficult to analyze. Since corrosion rates are very high at pH = 12 the polarization resistance, which is defined as the d.c. limit, (R_2 in Table IV) is very low. At -1000 mV a semicircle in the complex plane with a blocking capacitor at low frequencies is found and at -800 mV a negative going second semicircle is indicated. Since no CERT have been performed for Al 7075, the impedance data will not be discussed in greater detail.

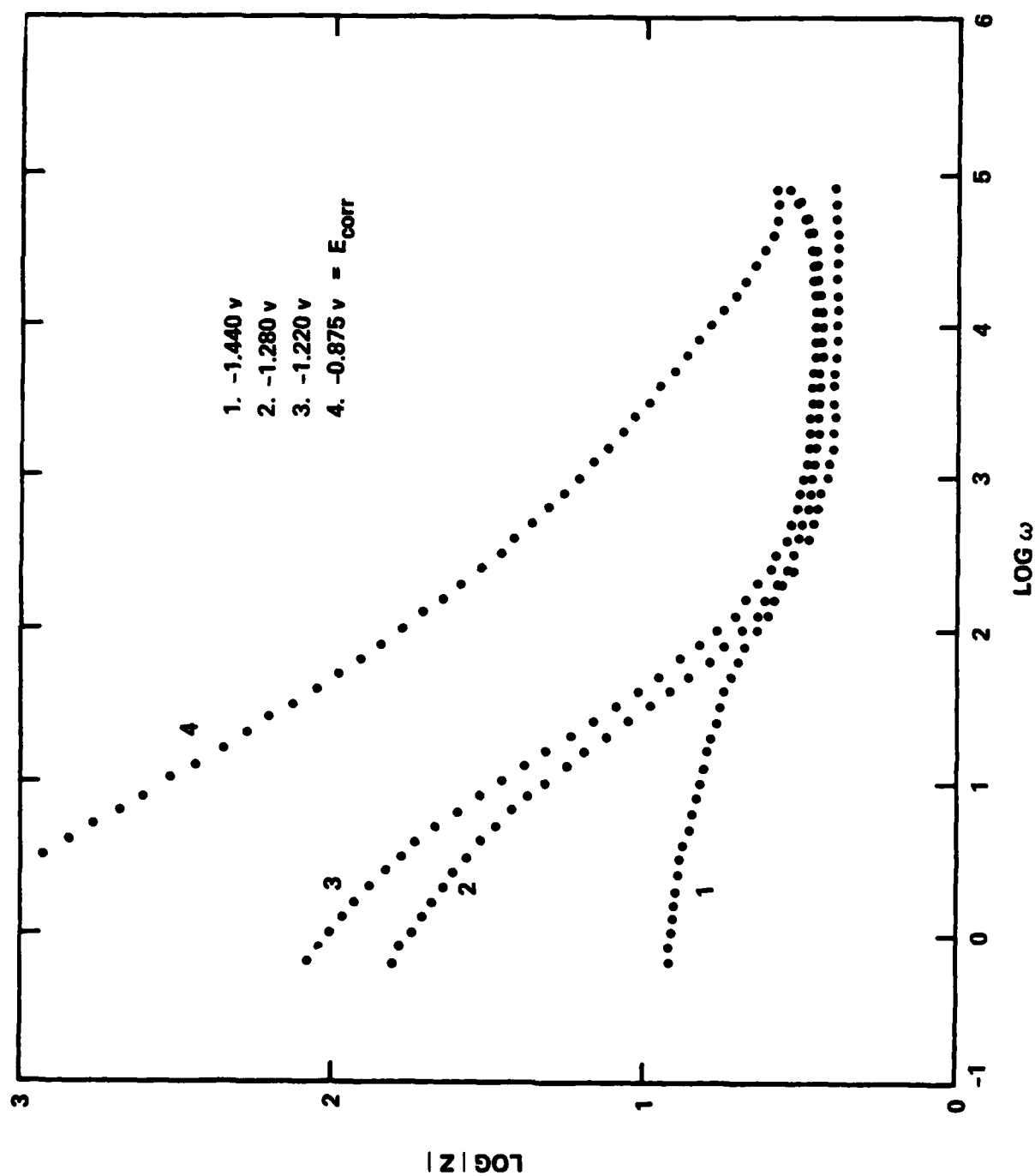


Fig. 14 Bode-plots for Al 7075-T6 (RCE) in neutral 1M NaCl, $T = 21^\circ\text{C}$ as a function of potential.

Table IV
A.C. Impedance Parameters for Al 7075 in 1 M NaCl

pH	E (mV vs SCE)	R ₁ (ohm)	C ₁ (μF)	R ₂ (ohm)	C ₂ (μF)	R ₀ (ohm)	DC	I _d c. (mA)
7	-875	n.a.	n.a.	>10 ⁴	500	4	E _{corr}	0
7	-1220	n.a.	n.a.	155	7100	3	c	0.43-0.41
7	-1280	n.a.	n.a.	105	~10 ⁴	3	c	0.75-0.73
7	-1440	n.d.	n.d.	6	~10 ⁴	3	c	8.2-10
12	-600	n.a.	n.a.	4	n.d.	3	tp	32-27
12	-800	48	n.a.	<0	6300	3	p	1.77-1.32
12	-1000	33	8000	∞	2750	3	p	2.04-1.43
12	-1200	n.a.	n.a.	>100	~10 ⁴	3	a→p	2.78-2.12
12	-1400	n.a.	n.a.	6	~10 ⁴	3	E _{corr}	0-2.1

n.a. = not applicable, only one relaxation process.

n.d. = not determined, broad relaxation.

c = cathodic

tp = transpassive

p = passive

a→p = active-to-passive.

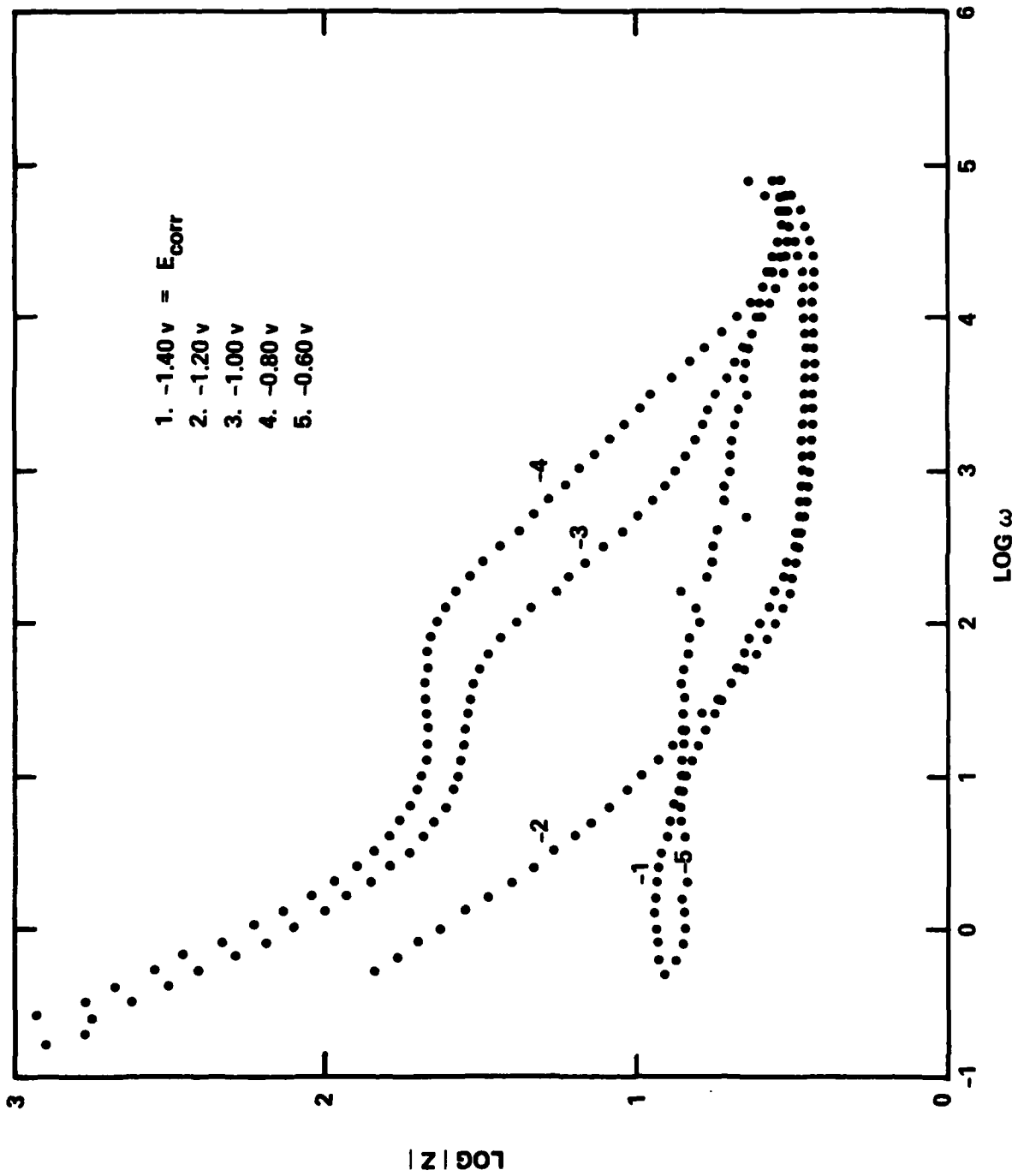


Fig. 15 Bode-plots for Al 7075-T6 (RCE) in 1M NaCl, pH = 12 as a function of potential.

3.3 CERT - Results

Figure 16 shows the stress vs strain curves for C1117 steel in mineral oil and in 1 N Na_3PO_4 , pH 4 at $E = 0$ mV vs SCE. The specimens in the electrolyte shows a somewhat reduced strength and breaks at a slightly lower strain, 57 mils (0.14 cm) as opposed to 59 mils (0.15 cm) for the specimen in oil. The a.c. impedance which was recorded continuously during CERT, was analyzed in greater detail at the four points indicated in Fig. 16. They include (1) the elastic region, (2) the point of maximum load where the specimen has yielded, (3) the region of high plastic deformation and, (4) the point just before failure.

The mechanical behavior of the material at various applied potentials in the two electrolytes studied was characterized using its elongation, percent reduction in cross sectional area (% RA), and time-to-failure. The corresponding results appear in Table V for the CERT performed for C1117 in phosphate electrolyte, carbonate electrolyte, in oil and in air. The steel in 1 N Na_3PO_4 showed a reduced strength at about 0 mV as judged by the % RA (Fig. 17). This corresponds to the potentiodynamic results (Figs. 2 - 6) from which a region of susceptibility to SCE was estimated which ranged from 0 to +250 mV.

3.3.1 Carbonate Solutions

The specimens in the carbonate/bicarbonate electrolyte show enhanced reduction in area as compared to behavior in oil over the entire potential range (Table V and Fig. 18). Some suggestion of more enhanced SCE susceptibility exists for the steel in carbonate/bicarbonate at potentials between -750 and -650 mV (Fig. 18).

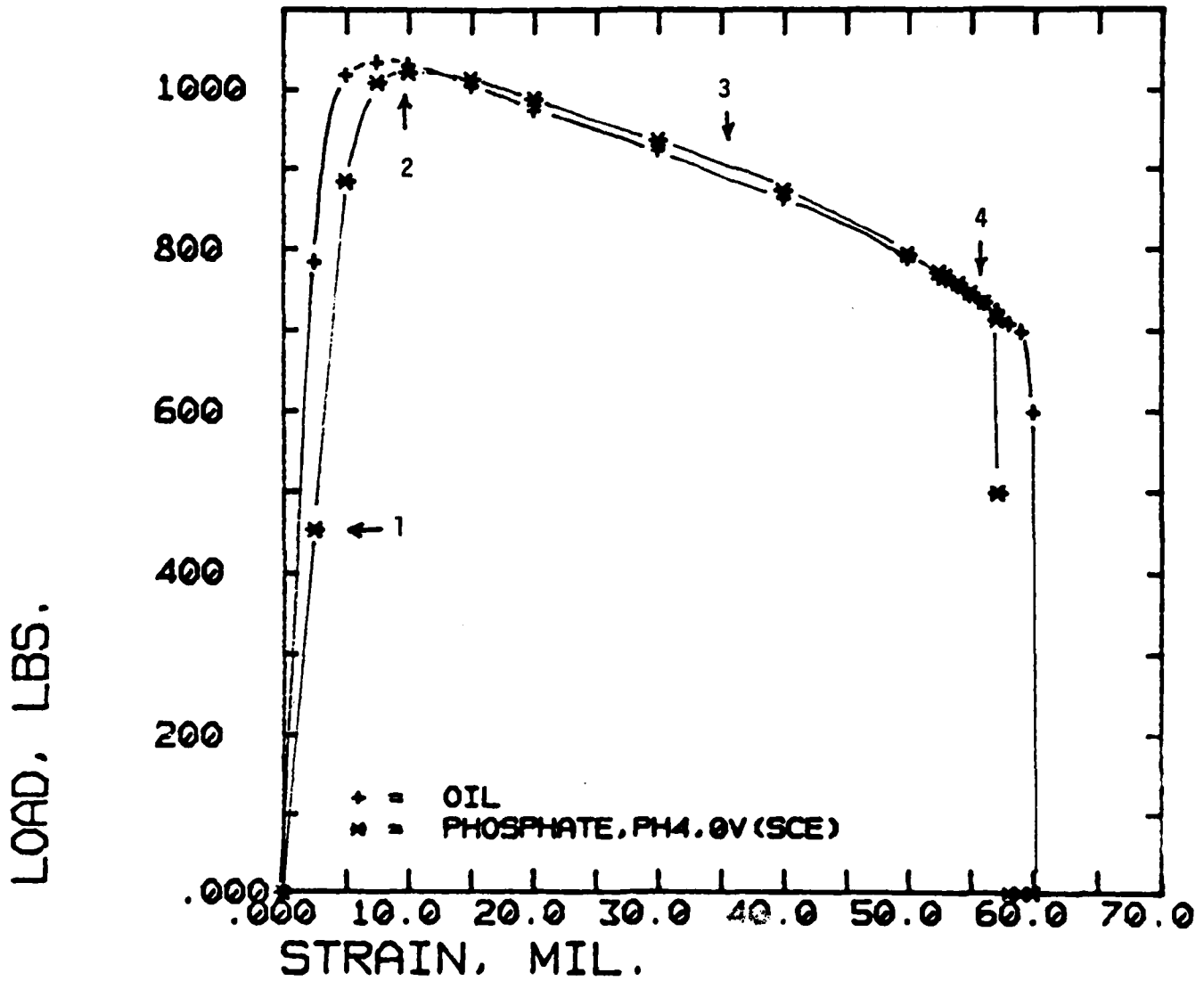


Fig. 16 Typical stress/strain curves for C1117 in 1N Na_3PO_4 and in mineral oil.

Table V
Results of Constant Extension Rate Testing

E (mV)	Elong. (in)	% RA	Time to Failure (h)
<u>I. 1N Phosphate, pH 4, 21°C</u>			
-400	0.0575	58	13.98
-200	0.0618	58	14.05
-150	0.0560	59	14.45
0	0.0570	47	13.29
+100	0.0569	58	14.35
+200	0.0575	56	14.88
+400	0.0605	58	14.03
<u>II. 1N Carbonate/0.1N Bicarbonate, 70°C</u>			
-750	0.0513	48	13.24
-750	0.0533	46	14.14
-690	0.0450	48	13.39
-640	0.0525	48	13.47
-200	0.0483	48	13.21
<u>III. Blank</u>			
oil	0.0590	59.3	
air		60.0	

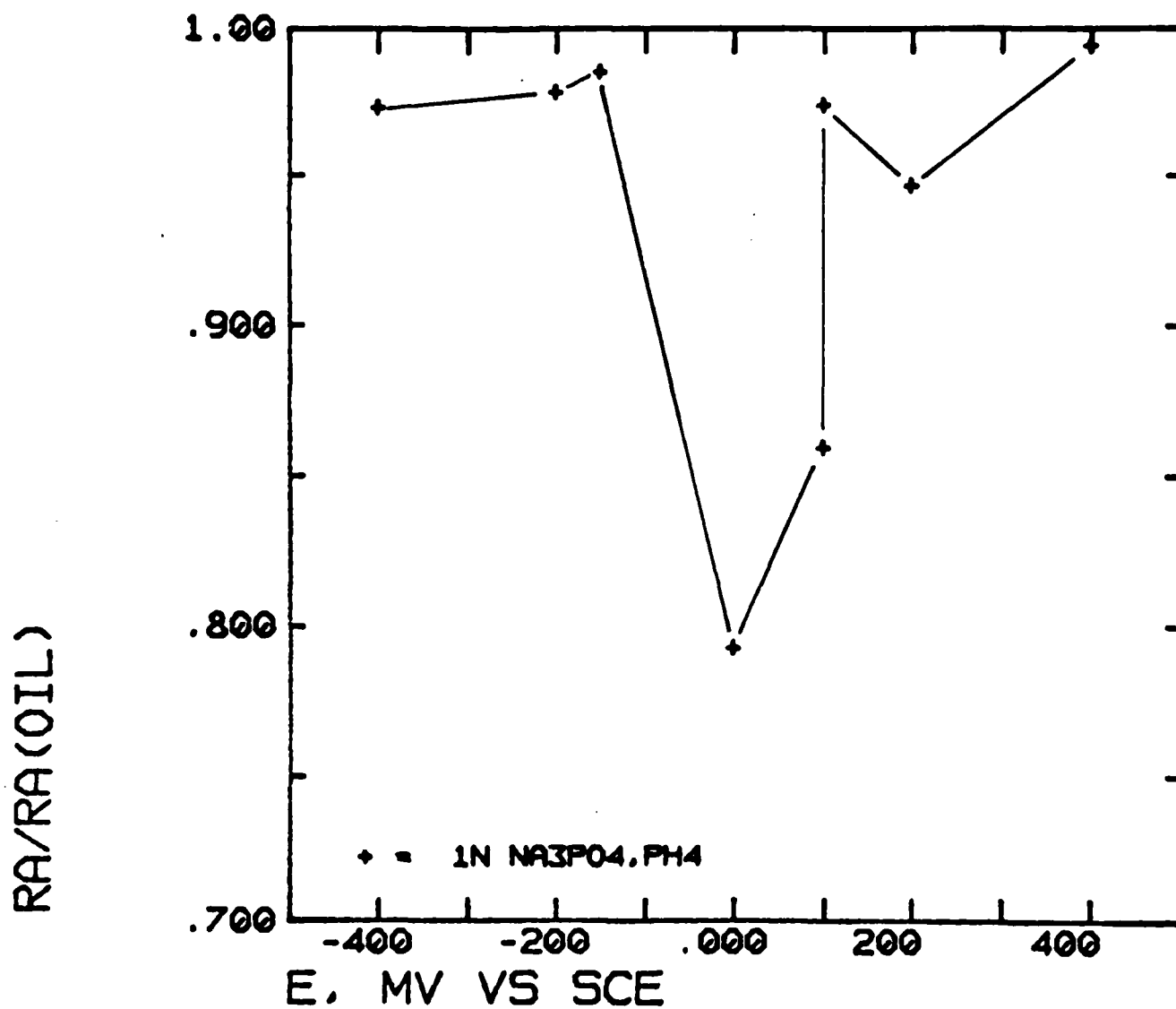


Fig. 17 Relative reduction in area (RA) for C1117 steel in 1N Na₃PO₄, pH = 4.

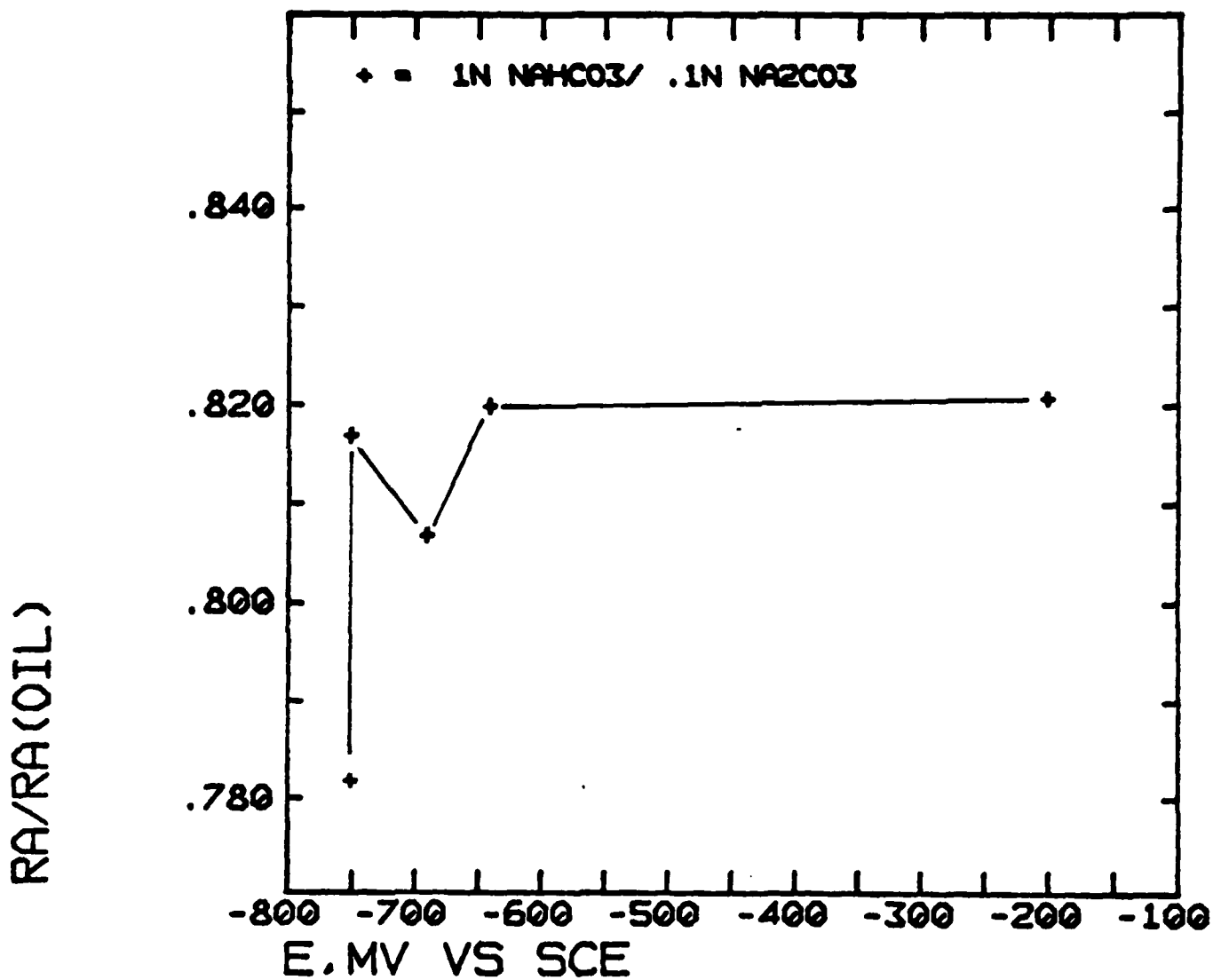


Fig. 18 Relative RA for C1117 steel in carbonate/bicarbonate solution.

Figure 19 shows the impedance data in the form of Bode plots at four potentials in 1N Na_3PO_4 , 21°C, pH 4, under conditions of elastic strain, point #1 (Fig. 16). At the active potential, $E = -400$ mV, the impedance response shows a frequency independent region at relatively high frequencies. This response typifies active dissolution and can be represented by a corrosion resistance in parallel with a double layer capacitance. A solution resistance in series with the double layer and corrosion resistance gives rise to a frequency independent region above $\omega = 10^4$ rad/s for all cases. At the more positive potentials, the impedance behavior is more complicated since films form at the electrode surface. At the passive potential of $E = +400$ mV, the electrochemical impedance shows nearly a ω^{-1} dependence at low frequencies corresponding to the capacitive behavior of the passive surface. At the intermediate potentials of 0 mV and +100 mV the impedance shows neither resistive nor capacitive behavior at the low frequencies. At +100 mV, the impedance tends toward ω^{-1} behavior only at very low frequencies. At 0 mV, a subtle plateau in the impedance curve appears between $\omega = 10^3$ and 10^2 rad/s. Similar behavior was observed for unstressed steel (Fig. 12). Strain influenced only the behavior of the specimen polarized at 0 mV, for which at high strains, this plateau region of the impedance disappeared. The plot of phase angle vs $\log \omega$ in Fig. 20 provides a more sensitive means of observing this effect. As the plateau disappears with higher strain a high frequency maximum in the phase angle between 10^3 and 10^4 rad/s (0.0025" and 0.010") gives way to a shoulder at frequencies below 10^2 rad/s (0.035" and 0.047") in Fig. 20.

3.3.2 Carbonate Solutions

Some similarities in the electrochemical impedance of C1117 steel in 1N Na_3PO_4 exist for the steel in 1N carbonate/0.1 N bicarbonate at 70°C under deaerated conditions. Figure 21 shows the Bode plots for this case. No d.c. limit was observed for the potentials between -750 mV and -200 mV. Capacitive response occurs for the specimens polarized at -640 mV and -200 mV. However, the capacitive behavior at -200 mV can result from a film which is thicker by a factor of 100 than that produced at -640 mV based on the assumption that dielectric films having the same dielectric constant determine the capacitive

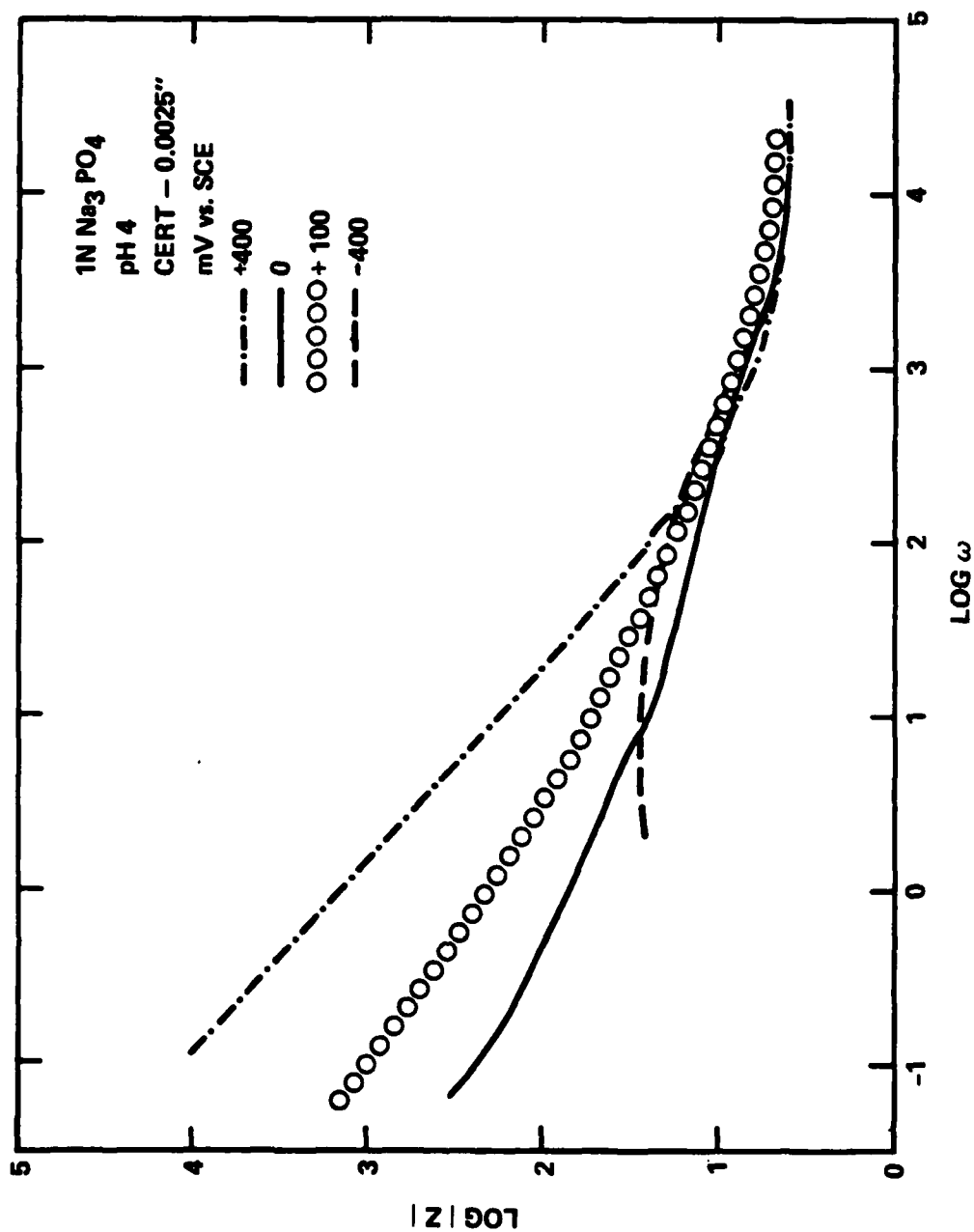


Fig. 19 Bode plots for C1117 steel in 1N Na₃PO₄, pH = 4, under elastic strain at -400, 0, 100 and 400 mV.

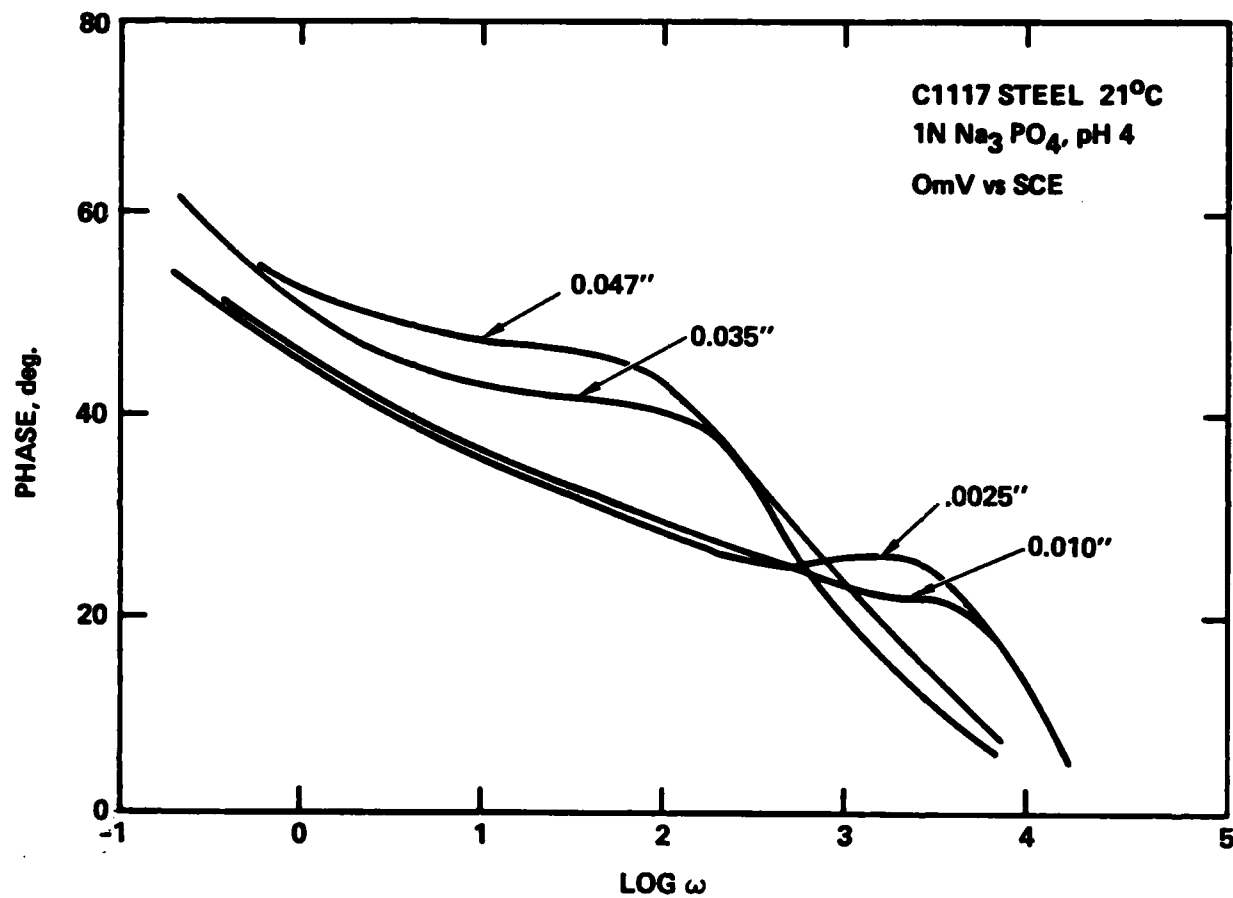


Fig. 20 Phase angle changes resulting from straining C1117 steel in 1N Na₃PO₄ at 0 mV.

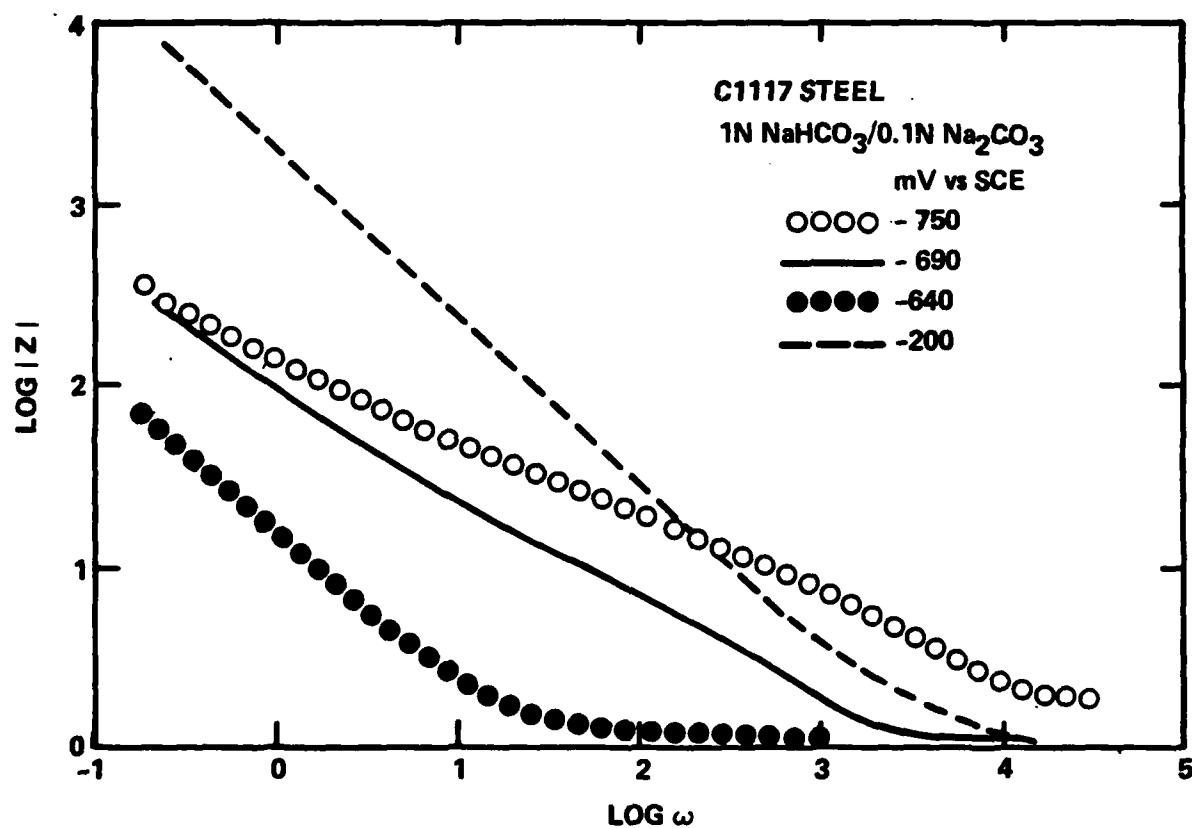


Fig. 21 Bode plots for C1117 steel in 1 N Na₂CO₃/0.1 N NaHCO₃ at 70°C under elastic strain.

impedance at these two frequencies. At -750 mV and -690 mV the electrochemical impedance shows neither purely capacitive nor resistive behavior over the entire observed potential region. At low frequencies and with no plastic strain, the impedance spectra for the specimens at -750 mV and -690 mV show a gradual approach to ω^{-1} behavior. At frequencies above 10^2 rad/s a relatively high impedance behavior results which does not fit the extrapolation of an assumed low frequency capacitance. An additional element lies in series with the solution resistance and capacitance. In addition, this region in the impedance spectra between $\omega = 10^2$ and 10^4 rad/s shows substantial changes under plastic strain of the material as shown by the dependence on strain of the phase angle spectra for -690 mV and -750 mV (Figs. 22 and 23). For the tensile specimen at -690 mV, the impedance between $\omega = 10^2$ and 10^3 rad/s shows a phase angle of 45° under elastic conditions. Upon straining, the electrochemical response becomes more dissipative as evidenced by a lowering of the phase angle in the $10^2 - 10^3$ rad/s region to below 30° directly before failure (Fig. 22). For the tensile specimen polarized to -750 mV a maximum in phase angle occurs above $\omega = 10^3$ rad/s under elastic strain. However, at yield this maximum shifts to lower frequencies and disappears upon very large strain (Fig. 23).

4.0 DISCUSSION

The present effort has centered on an evaluation of electrochemical techniques which have been suggested to be useful for determining the potential regions where steel could be susceptible to SCC. Parkins et al.^(2,8,9) have used the differences in current flow in fast and slow anodic polarization scans in the active-to-passive and the passive region to determine the critical potential range. Armstrong and Coates⁽³⁾ have determined a time constant τ for passivation for the same purpose by analyzing ac impedance data. Where a maximum for τ is observed, maximum susceptibility to SCC is expected and it is argued that at this potential the most unfavorable correlation between metal dissociation and repassivation kinetics exists which makes SCC possible.

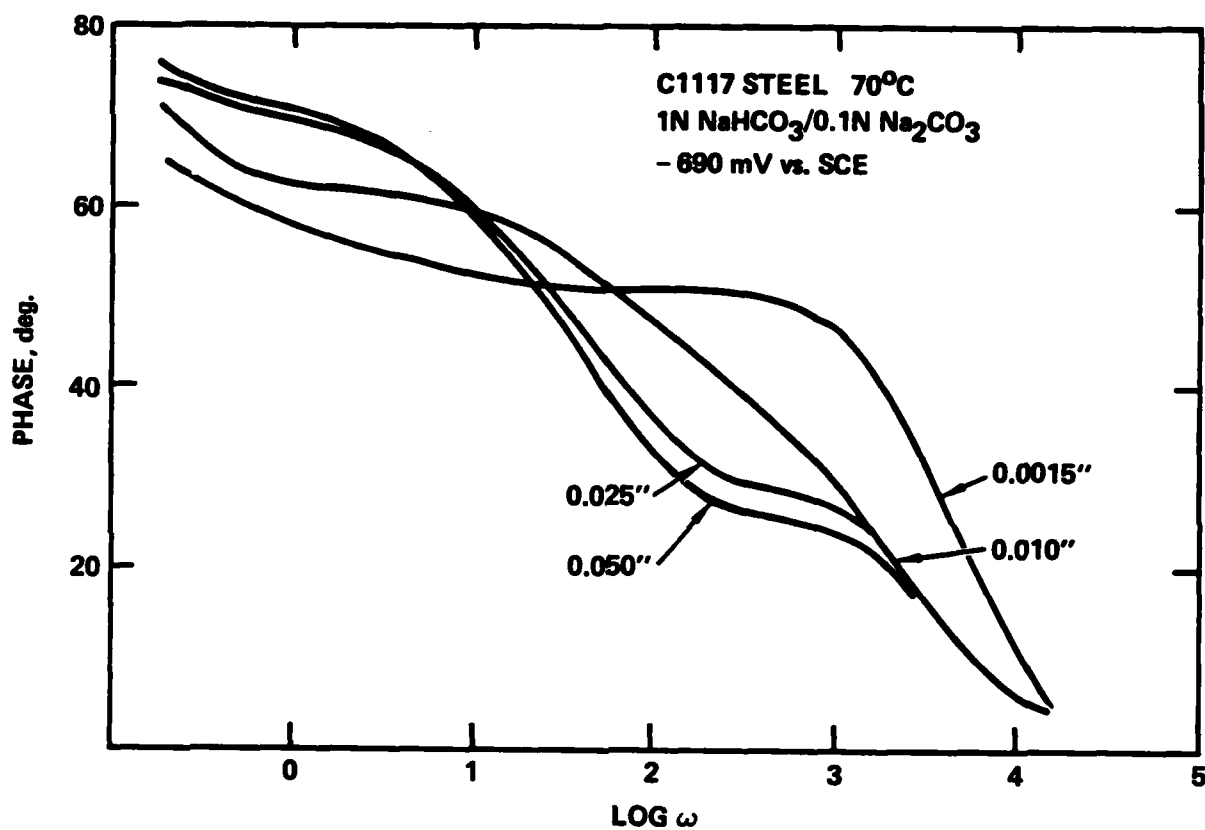


Fig. 22 Phase angle plots for C1117 steel in 1N Na₂CO₃/0.1 N NaHCO₃ at -690 mV at different strains.

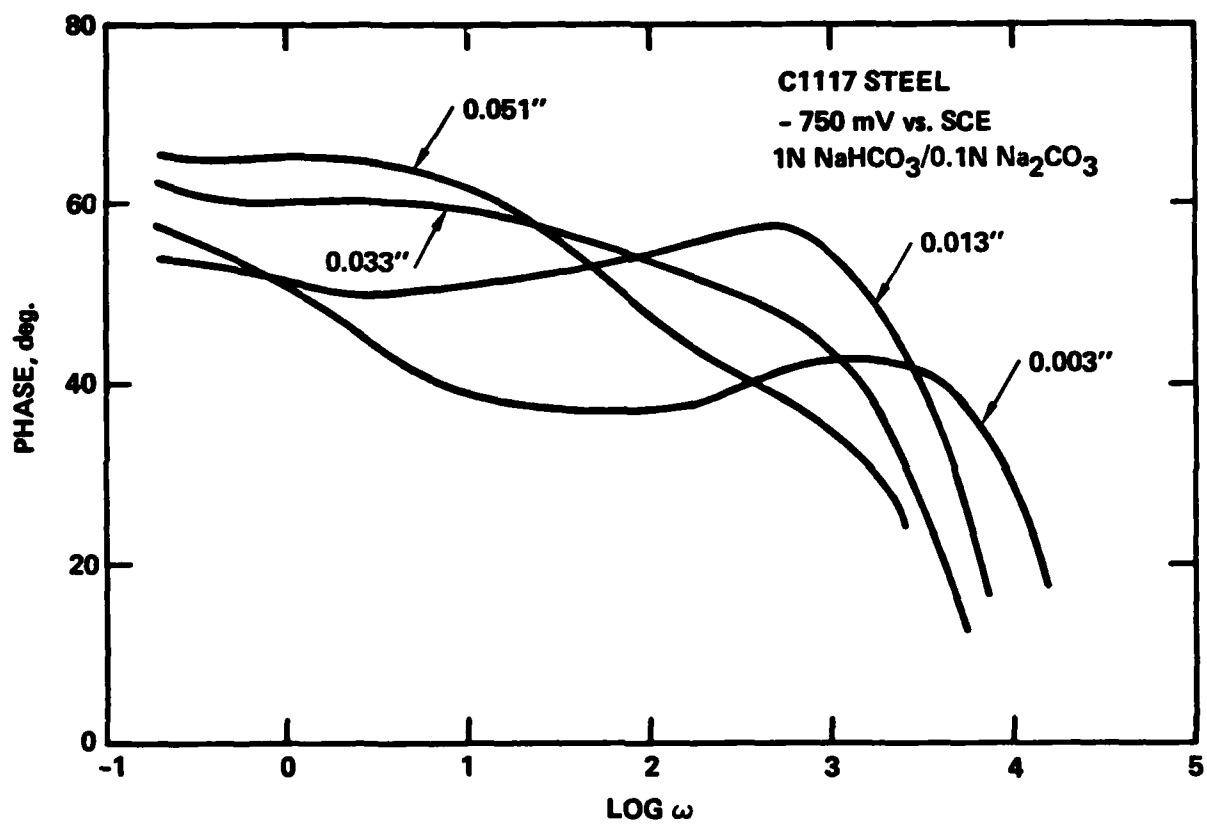


Fig. 23 Phase angle plots for C1117 steel in 1N Na₂CO₃/0.1 N NaHCO₃ at -750 mV at different strains.

The criterion of Parkins has been used to determine the SCC regions for C1117 steel in 1N Na_3PO_4 , pH = 4 at 21°C and in 1.0 N $\text{NaHCO}_3/0.1$ N Na_2CO_3 at 70°C for subsequent CERT. A principal error in Parkins' approach is the neglect of the ohmic drop which causes a distortion of the polarization curves and leads to a scan rate which is not constant throughout the potential range studied. Since the true potential of the test electrode surface E_{WE} is the difference between the applied potential E_0 and the ohmic drop $\eta_\Omega = IR_\Omega$, the real scan rate dE_{WE}/dt equals:

$$\frac{dE_{WE}}{dt} = \frac{dE_0}{dt} - \frac{d\eta_\Omega}{dt} \quad (2)$$

This means that in the active dissolution region the real scan rate is less than the applied scan rate, while in the active-to-passive transition region the reverse is true. While these effects are important in the determination of the "true" polarization curve, experimentally not much difference was found in the calculated regions of susceptibility to SCC (Fig. 3).

In 1 N Na_3PO_4 the present electrochemical results do not agree with those of Parkins et al.⁽⁹⁾ who determined a cracking region of -100 mV to -470 mV vs SCE, while in the present case a cracking range of 0 to +250 mV was found. The suggestion by Parkins et al.⁽⁹⁾ that 1N Na_3PO_4 and 1N Na_2HPO_4 cause cracking, but not 1 N NaH_2PO_3 (all at pH = 4) because increased corrosion without passivation and without SCC was not confirmed in the present tests. Such an effect was very unlikely based on the similar chemistry of the three solutions.

A second approach to determine the cracking range is that of Armstrong⁽³⁾ who determined the time constant τ for passivation. It was found that true ac impedance data cannot be obtained in the active-to-passive transition region, because of continuous change of the current at a constant applied potential until passivation occurred. Very rapid impedance measurements at a minimum number of frequencies and at minimum measuring time gave results similar to those reported by Armstrong,⁽³⁾ but this method was not considered very reliable.

CERTs were carried out at an extension rate of $2.5 \cdot 10^{-6} \text{ s}^{-1}$ in order to duplicate Parkins' SCC results.⁽⁹⁾ The tests were performed in 1 N Na_3PO_4 , pH = 4, $T = 21^\circ\text{C}$ and in 1.0 N NaHCO_3 /0.1 N Na_2CO_3 at 70°C at constant potential with continuous recording of ac impedance spectra between 10 kHz and 30 mHz. Examination of the stress-strain curves, reduction in area, percent elongation and time to failure gave some indication of SCC; however, the effect was not very pronounced. In 1 N Na_3PO_4 SCC is indicated at about 0 mV, while in the carbonate solution the mechanical properties are reduced at all potentials as compared to CERT in mineral oil with a minimum at -700 mV which is in the active-to-passive transition region close to the current peak (Fig. 5). Since the current ratio in fast and slow sweeps was less than 100 (Fig. 5), a prediction of the SCC range was very difficult in this case. It is possible that the observed low susceptibility to SCC is due to the use of cold rolled C1117 steel. Parkins et al.⁽⁹⁾ state that similar results were obtained in phosphate solutions for a steel with a small amount of cold work ($\sim 1\%$) after hot rolling and a steel which was annealed 1 h at 950°C before use. The C-Mn steel used in the present study has a similar chemical composition as that used by Parkins⁽⁹⁾ and was used as received.

The ac impedance data do not show much change between the behavior at potentials where the steel is susceptible or non-susceptible to SCC. However, the fact that a second, high frequency relaxation phenomenon is observed at the potential of maximum susceptibility and appears to be influenced by applied stress, suggests that the impedance data can indeed give some information about the events leading to SCC. A model for the impedance behavior resulting from changes of surface structure and chemistry is given in the following.

Model for Electrochemical Impedance Behavior of C1117 Steel During CERT

The model schematically presented in Figs. 24 and 25 provides a consistent explanation of the impedance observed during the CERT. Under conditions of active dissolution, the impedance analog for the electrochemical response includes a parallel double layer capacitance, C and corrosion resistance, R_p , in series with the ohmic solution resistance R_Ω . The schematic of the response for

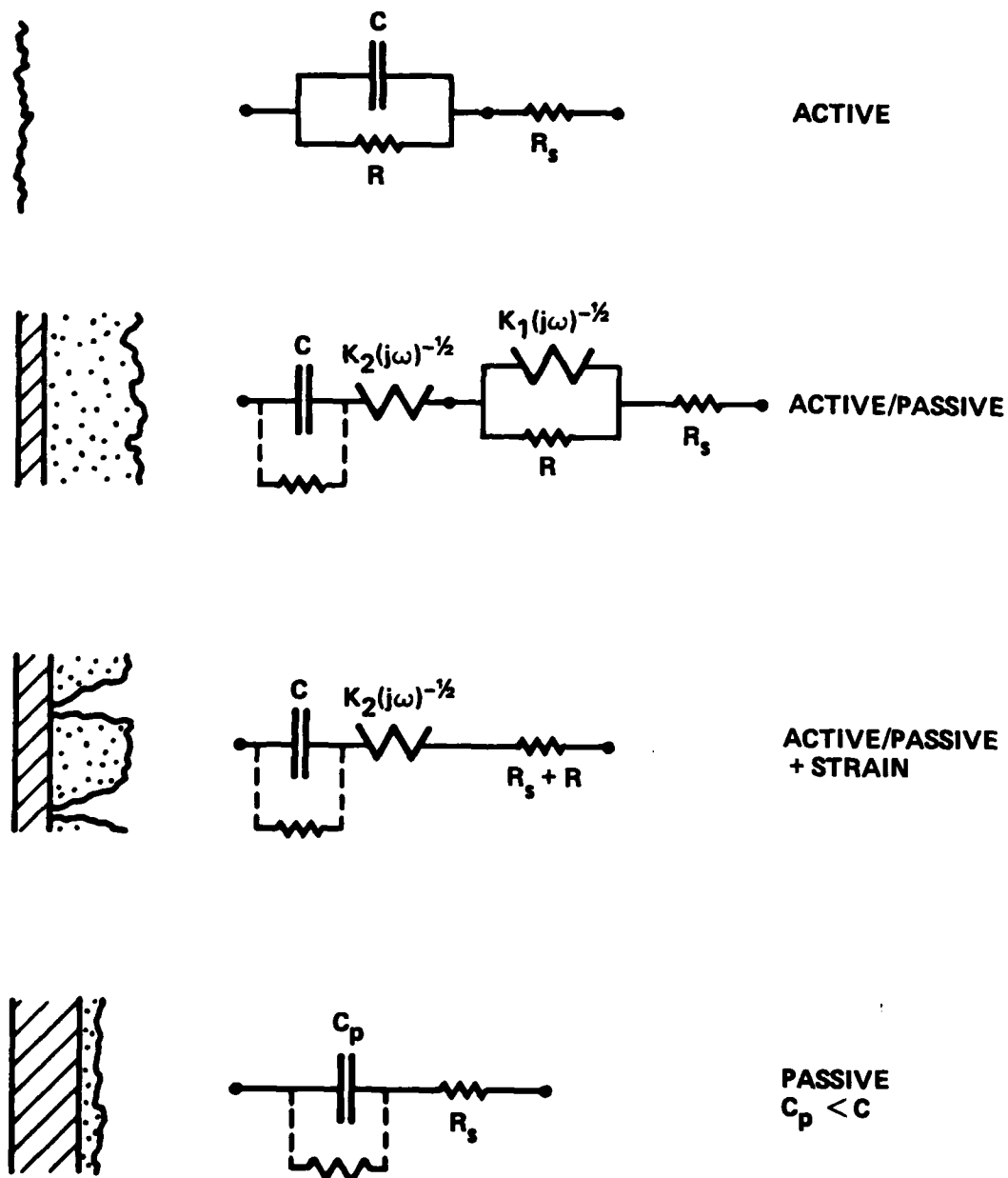


Fig. 24 Model for impedance of C-Mn steel. Circuit analogs of surface films.

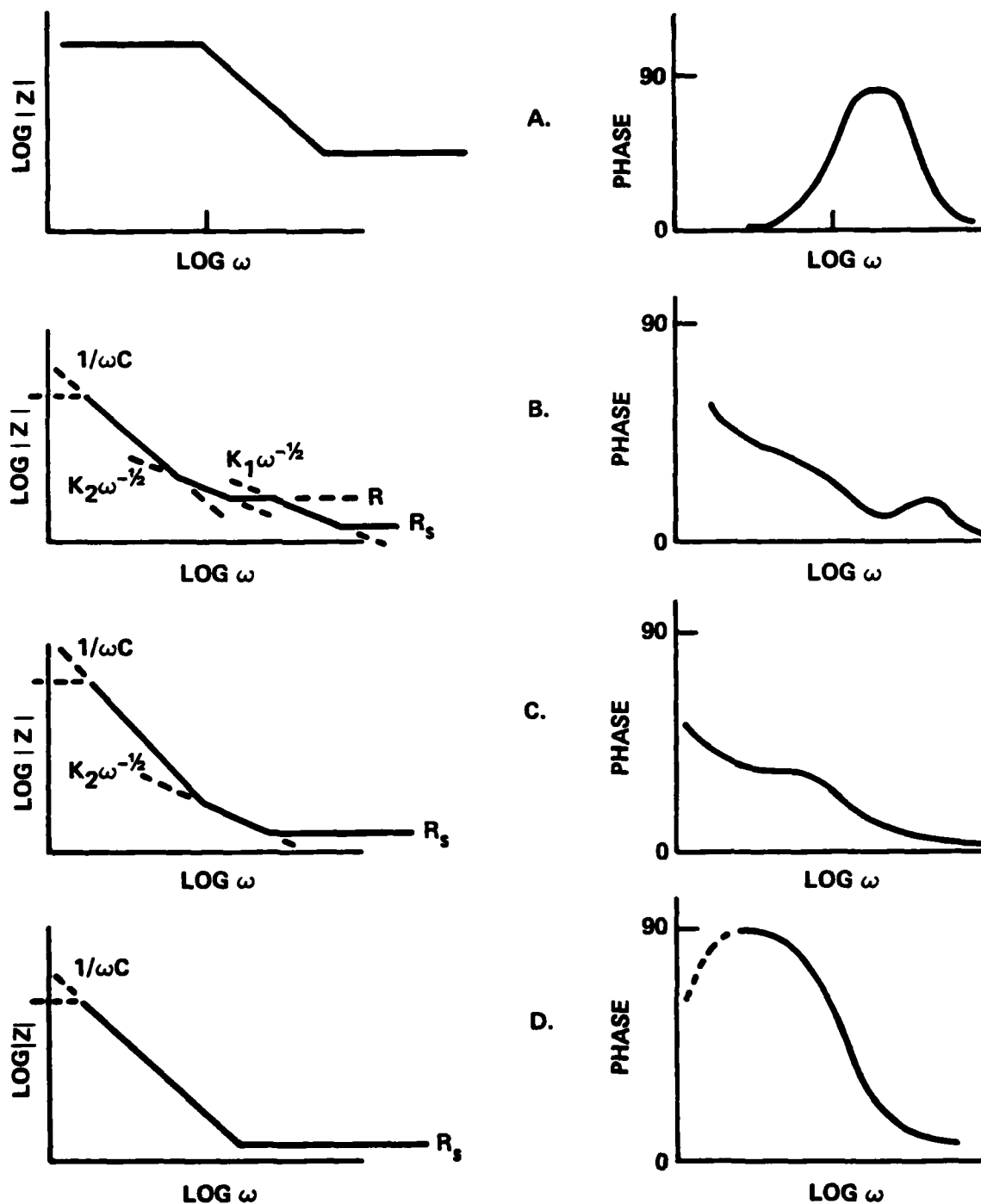


Fig. 25 Model for impedance of C-Mn steel. Schematic Bode plots for cases presented in Fig. 24.

this active case appears in the Bode-plots in Fig. 25a and the steel in 1N Na_3PO_4 at -400 mV demonstrates this behavior (Fig. 19).

For the active-to-passive transition region at steady state, the impedance results are consistent with the formation of a duplex film consisting of a porous outer precipitate layer and a thin heterogeneous inner layer. The partially protective inner film can be represented by a capacitor which shows substantial dissipation at high frequencies. It may be represented by a capacitor in series with a pseudo-Warburg element $K_2(j\omega)^{-1/2}$. The physical significance of the pseudo Warburg impedance comes from the heterogeneous and partial porous material of the inner layer. The outer layer results from a precipitation of corrosion products and shows mostly resistive behavior represented by R_p . The properties of the outer film also make it behave as a porous electrode giving rise to pseudo-Warburg behavior at high frequencies. The pseudo-Warburg of the outer film is represented by $K_1(j\omega)^{-1/2}$ (Fig. 24b). Figure 25b shows the impedance response for the active-to-passive case. The high frequency maximum in the phase angle also appears in Fig. 25b and exemplifies the response of the steel in carbonate/bicarbonate at -690 and -750 mV and for steel in pH = 4 phosphate at 0 mV (Figs. 22, 23 and 20, respectively).

With strain, however, mechanical disruption of the outer film provides lower resistance paths which bypass the $K_1(j\omega)^{-1/2}$ impedance and effectively eliminate this element (Fig. 24c), and the high frequency phase angle maximum (Fig. 11c). A lower frequency shoulder in the phase angle results from the nature of the inner film which behaves as $K_2(j\omega)^{-1/2}$ at high frequencies, but follows a capacitive response $(j\omega C)^{-1}$ at low frequencies (Fig. 25c). The steel specimens at -690 mV and -750 mV in carbonate/bicarbonate and at 0 mV in 1N Na_3PO_4 show this shift in phase angle at high strains as illustrated in Figs. 20, 22 and 23, respectively.

At passive potentials the electrode behaves as a capacitor C_p in series with a solution resistance R_Ω thereby giving rise to ω^{-1} behavior down to low frequencies as in the case for the steel at high anodic overpotentials in both electrolytes (Figs. 19 and 21). The resulting capacitance, C_p , may be substantially smaller than those observed for the inner films in the active-to-passive transition regions due to substantial film growth.

5.0 RECOMMENDATIONS FOR FUTURE WORK

The present study has shown that the electrochemical impedance behavior of C-Mn steel tensile specimen in 1N Na_3PO_4 and in alkaline carbonate electrolytes is consistent with a model of a surface composed of two films. An inner film shows capacitive behavior in the active-to-passive and passive regions. The inner film becomes thicker in the passive regions and dominates the impedance response. In the active-to-passive region a thick precipitated film exists outside the inner film. This precipitate film becomes highly conductive with high strain. The inner film in the active-to-passive region is less protective and shows greater electrical loss than that in the passive region.

Future work should concentrate on developing an experimental approach for determination of the mechanical impedance $Z_m^{(1)}$ which is defined as $Z_m = \Delta\sigma(j\omega)/\Delta I(j\omega)$, where $\Delta\sigma$ is a small amplitude cyclic stress superimposed over a constant stress and ΔI is the resulting AC current. These results should be compared with the electrochemical impedance Z_{e1} determined at the same constant stress without $\Delta\sigma$. Such measurements should be performed for the C-Mn steel, a high strength steel (such as 4340) and aluminum 7075 under potentiostatic control in the elastic and plastic region. The potential region where these materials are susceptible or immune to SCC as determined by CERT should be explored. The characteristic time constants for Z_m and Z_{e1} will be correlated with SCC susceptibility. By observing the relaxation of the electrode processes which couple to surface deformation it should be possible to determine directly the mechanical and electrochemical coupling modes which may relate to the very early stages of SCC. A correlation of the mechanical and electrochemical coupling to SCC could possibly lead to the development of novel methods of NDE and a capability to predict SCC susceptibility from a relatively rapid electrochemical test.

In future studies, attention should be paid also to corrosion fatigue (CF) in a similar manner. The mechanical and electrochemical impedances should be determined for steels and Al alloys and correlations should be established between CF behavior and impedance characteristics.

Finally, the results for SCC and CF should be analyzed to determine the feasibility of using electrochemical and mechanical impedance techniques to determine CF and SCC susceptibility of different materials and to make material selections.

REFERENCES

1. A. Roelandt and J. Vereecken, Surf. Techn. 9, 347 (1979).
2. R.N. Parkins, Corr. Sci. 20, 147 (1980).
3. R.D. Armstrong and A.C. Coates, Corr. Sci. 16, 433 (1976).
4. F. Mansfeld and J.V. Kenkel, Corrosion 32, 380 (1976).
5. K. Schwabe, W. Oelssner and H.D. Suschke, Prot. Metals 15, 126 (1979).
6. F. Mansfeld, M.W. Kendig and S. Tsai, "Corrosion Kinetics in Low Conductivity Media, I. Iron in Natural Waters," Corr. Sci. (in press).
7. F. Mansfeld, Corrosion 37, 301 (1981).
8. J.M. Sutcliffe, R.R. Fessler, W.K. Boyd and R.N. Parkins, Corrosion 28, 313 (1972).
9. R.N. Parkins, N.J.H. Holroyd and R.R. Fessler, Corrosion 34, 253 (1978).

